RESEARCH ARTICLE SUMMARY

BIOMEDICINE

Neutrophil extracellular traps target senescent vasculature for tissue remodeling in retinopathy

François Binet, Gael Cagnone, Sergio Crespo-Garcia, Masayuki Hata, Mathieu Neault, Agnieszka Dejda, Ariel M. Wilson, Manuel Buscarlet, Gaelle Tagne Mawambo, Joel P. Howard, Roberto Diaz-Marin, Celia Parinot, Vera Guber, Frédérique Pilon, Rachel Juneau, Rémi Laflamme, Christina Sawchyn, Karine Boulay, Severine Leclerc, Afnan Abu-Thuraia, Jean-François Côté, Gregor Andelfinger, Flavio A. Rezende, Florian Sennlaub, Jean-Sébastien Joyal*, Frédérick A. Mallette*, Przemyslaw Sapieha*

INTRODUCTION: Vision provides a critical survival advantage but requires a tight coupling between neuronal energy demands and their vascular supply. The degeneration and consequent aberrant regrowth of retinal vasculature is the hallmark of diseases such as diabetic retinopathy, retinopathy of prematurity, and age-related macular degeneration, which collectively are the most common causes of loss of sight in industrialized countries. Although considerable effort has been devoted to understanding how diseased blood vessels form, relatively little is known of the processes at play during late stages of pathological angiogenesis when blood vessels remodel and subsets of diseased vasculature regress.

RATIONALE: The retina is part of the central nervous system and thus has limited regenerative capacity. A relative exception to this rule are retinal blood vessels, which have a greater propensity to remodel depending on metabolic demand. We investigated the cellular mechanisms activated during the remodeling and regression of pathological blood vessels in retinopathy. We focused on a mouse model of oxygen-induced retinopathy, which has distinct and timed phases of vascular degeneration, neovascularization, and vascular regression. Our findings were verified in human patients with proliferative diabetic retinopathy. Understanding how diseased blood vessels remodel and yield functional networks has the potential to lead to strategies that enhance vascular normalization and helps to explain why retinas in certain patients have the propensity to repair themselves more readily than others.

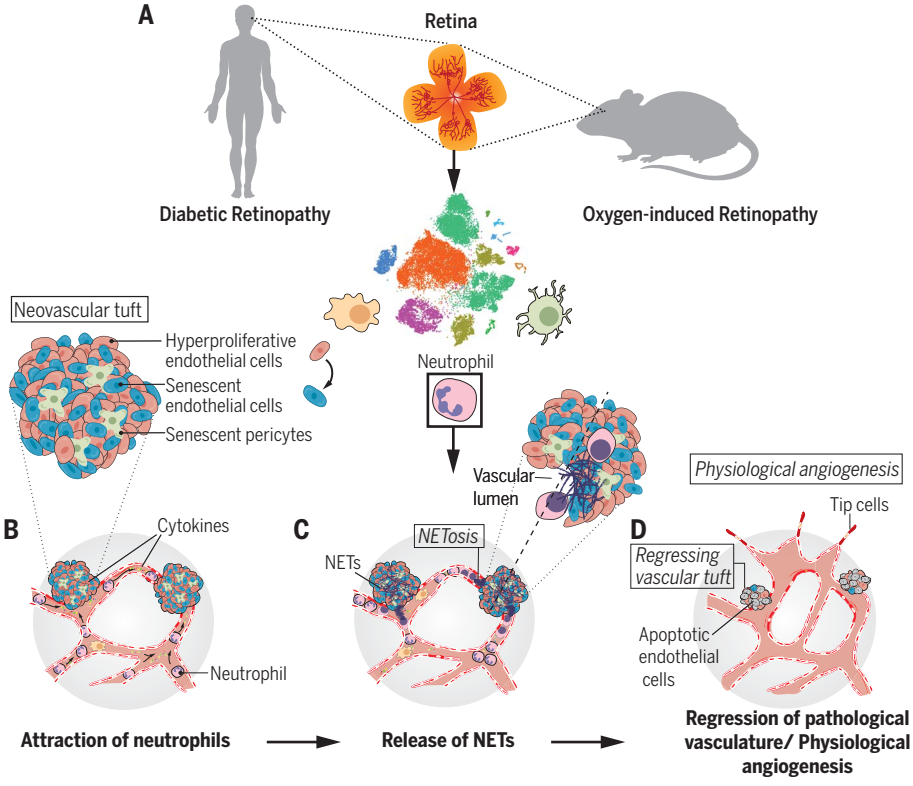

Senescent blood vessels trigger neutrophil extracellular traps in retinopathy. (**A**) Human samples and a mouse model were used to elucidate mechanisms of vascular remodeling in retinopathy. (**B**) Upon rapid proliferation, vascular cells in pathological tufts triggered pathways of cellular senescence, leading to cytokine secretion and the recruitment of neutrophils. (**C**) Factors secreted by senescent cells triggered NETosis. (**D**) NETs promoted the removal of senescent endothelial cells, ultimately leading to regression of pathological angiogenesis and promoting the regeneration of functional vessels.

RESULTS: We found that vascular remodeling in retinopathy is associated with bouts of sterile inflammation and tardy recruitment of neutrophils, an immune population typically associated with a first wave of invading leukocytes. We observed that, after rapid proliferation, vascular endothelial cells in diseased blood vessels engaged molecular pathways shared with aging and cellular damage that lead to cellular senescence. Senescent vascular units then released a secretome of cytokines and factors that attracted neutrophils and triggered the production of neutrophil extracellular traps (NETs). Through extrusion of NETs, neutrophils eliminated diseased senescent vasculature by promoting its apoptosis. By crippling the ability of neutrophils to produce NETs by genetically removing the peptidyl arginine deiminase type IV (PAD4) enzyme, clearance of senescent cells was impaired and regression of pathological angiogenesis compromised. Similar effects were observed with the neutrophil-depleting antibody anti-Ly6G or by pharmacological inhibition of the neutrophil receptor CXCR2.

CONCLUSION: We conclude that neutrophils, through the release of NETs, targeted pathological senescent vasculature for clearance and thus prepare the ischemic retina for reparative vascular regeneration. These findings imply that elimination of senescent blood vessels leads to beneficial vascular remodeling. Although cellular senescence is not necessarily synonymous with aging, our study may provide insight into a general mechanism in which senescent endothelial cells trigger NETosis and predispose to thrombotic events such as myocardial infarction, atherosclerosis, and stroke, which are typically seen in older populations. ■

The list of author affiliations is available in the full article online.
*Corresponding author. Email: mike.sapieha@umontreal.ca (P.S.); fa.mallette@umontreal.ca (F.A.M.); js.joyal@umontreal.ca (J.-S.J.)
Cite this article as F. Binet *et al.*, *Science* **369**, eaay5356 (2020). DOI: 10.1126/science.aay5356

READ THE FULL ARTICLE AT
https://doi.org/10.1126/science.aay5356

RESEARCH ARTICLE

BIOMEDICINE

Neutrophil extracellular traps target senescent vasculature for tissue remodeling in retinopathy

François Binet[1,2], Gael Cagnone[3,4], Sergio Crespo-Garcia[1,2], Masayuki Hata[1,2], Mathieu Neault[2], Agnieszka Dejda[1,2], Ariel M. Wilson[1], Manuel Buscarlet[2], Gaelle Tagne Mawambo[2], Joel P. Howard[3], Roberto Diaz-Marin[2], Celia Parinot[1], Vera Guber[1], Frédérique Pilon[1], Rachel Juneau[1], Rémi Laflamme[1], Christina Sawchyn[2], Karine Boulay[2], Severine Leclerc[3], Afnan Abu-Thuraia[5], Jean-François Côté[5], Gregor Andelfinger[3], Flavio A. Rezende[1], Florian Sennlaub[6], Jean-Sébastien Joyal[1,3,4,7]*, Frédérick A. Mallette[2,8]*, Przemyslaw Sapieha[1,2,9]*

In developed countries, the leading causes of blindness such as diabetic retinopathy are characterized by disorganized vasculature that can become fibrotic. Although many such pathological vessels often naturally regress and spare sight-threatening complications, the underlying mechanisms remain unknown. Here, we used orthogonal approaches in human patients with proliferative diabetic retinopathy and a mouse model of ischemic retinopathies to identify an unconventional role for neutrophils in vascular remodeling during late-stage sterile inflammation. Senescent vasculature released a secretome that attracted neutrophils and triggered the production of neutrophil extracellular traps (NETs). NETs ultimately cleared diseased endothelial cells and remodeled unhealthy vessels. Genetic or pharmacological inhibition of NETosis prevented the regression of senescent vessels and prolonged disease. Thus, clearance of senescent retinal blood vessels leads to reparative vascular remodeling.

The propensity of a tissue to rapidly repair and remodel after injury or in pathology dictates fitness and functional recovery. An example occurs in ischemic retinopathies such as retinopathy of prematurity (ROP) and diabetic retinopathy (DR). Collectively, these diseases are the primary causes of blindness in pediatric and working-age populations in developed countries, and for DR, affect >100 million people worldwide (*1*–*6*). Both diseases are characterized by an initial loss of retinal vascular supply and compromised nutrient and oxygen delivery (*7*–*9*). The ensuing tissue hypoxia-ischemia triggers the release of angiogenic and inflammatory factors that potentiate vascular growth (*10*). However, these neovessels fail to regenerate into the ischemic retina and are instead misdirected toward the vitreous part of the eye; they are leaky, senescent, and in severe instances, become fibrotic and lead to blinding retinal detachment (*3*, *5*, *11*).

In ROP, the pathological vessels driving disease often regress and sight is spared (*5*, *6*, *12*). This is in part illustrated by the fact that patients with ROP often spontaneously recover and of the estimated 14,000 to 16,000 infants that are initially affected by ROP each year in the United States, ~90% do not necessitate treatment. Of the ~1500 infants that do require treatment, ~1/3 will become legally blind (*12*). In DR, spontaneous regression of neovascularization (NV) has been reported (*13*, *14*), albeit less frequently given that upon diagnosis, standard of care calls for immediate pan-retinal photocoagulation (*15*), anti–vascular endothelial growth factor (anti-VEGF) therapy (*16*), or other treatments such that physiological regression is not readily monitored. The mechanisms mediating spontaneous regression and normalization of pathological retinal vessels in these conditions are poorly understood.

Physiological regression and remodeling of vascular networks occur during the transition from fetal to neonatal life in various tissues such as the hyaloid vasculature in the eye (*17*–*19*) and ductus arteriosus (*20*), as well as in the female reproductive system during endometrial maturation (*21*). Failure of proper vascular regression leads to diseases such as persistent fetal vasculature and familial exudative vitreoretinopathy (*22*), patent ductus arteriosus (*23*), and suboptimal reproductive performance (*24*). In pathology, less is known about the endogenous mechanisms that drive vascular remodeling. Anti-VEGF therapies in tumors either induce apoptosis of endothelial cells (ECs) [reviewed in (*25*)] or normalize blood vessels by pruning tortuous, leaky vessels not covered by pericytes (*26*), allowing enhanced delivery of cytotoxic factors in combination therapies (*27*). Vascular remodeling is therefore an evolutionarily adaptive mechanism critical to development and regeneration after tissue injury. Here, we sought to understand how diseased retinal blood vessels remodel in retinopathies and consequently influence prognosis.

Results

Vascular remodeling in retinopathy is associated with sterile inflammation

To investigate the mechanisms involved in pruning of pathological vasculature in retinopathies, we first used a mouse model of oxygen-induced retinopathy (OIR) (*28*) that yields ischemic avascular zones followed by preretinal NV similar to that observed in proliferative DR (PDR) and ROP (*28*). Mouse pups were exposed to 75% oxygen from postnatal day 7 (P7) to P12 to induce vaso-obliteration and returned to ambient air, where maximal preretinal NV occurs at P17, followed by a phase of vascular regression (Fig. 1A). To gain insight into the physiological processes occurring during NV (P12 to P17 of OIR), vascular remodeling and regression (from P17 of OIR), we first performed transcriptome analyses using bulk-RNA sequencing. Enrichment analysis using gene sets from the Gene Ontology (GO) Consortium at P14 of OIR revealed the highest expression of transcripts linked to endoplasmic reticulum homeostasis (Fig. 1B, left), which is consistent with previous findings (*11*, *29*). At the tipping point from maximal pathological angiogenesis to normalization of vasculature at P17 of OIR, we observed transcript enrichment primarily in processes related to inflammation and, more precisely, activation of the innate immune system (P17 of OIR) (Fig. 1B, right).

To tease out the primary contributors of the sterile inflammatory response associated with vascular remodeling in the late stages of retinopathy, we heightened resolution by performing droplet-based single-cell RNA sequencing (Drop-seq) (*30*) of retinas during OIR. Principal components analysis and a t-distributed stochastic neighbor embedding (t-SNE) plot of different clustered retinal cell types with similar transcriptional profiles revealed the typical cell populations present in the retina, including neurons, glial cells, and vascular cells (Fig. 1C, left inset, and fig. S1A). Among the populations defined as immune cells, we identified five independent subclusters (Fig. 1C, middle inset). One subpopulation (cluster 3) was found to be especially enriched at P17 of OIR (Fig. 1C, right inset) and corresponded to disease-associated leukocytes defined using the SingleR tool (*31*) (fig. S1B). Gene-set variation analysis (GSVA) revealed that this group of

[1]Departments of Ophthalmology and [2]Biochemistry and Molecular Medicine, Maisonneuve-Rosemont Hospital Research Centre, University of Montreal, Montreal, Quebec H1T 2M4, Canada. [3]Departments of Pediatrics and [4]Pharmacology, Centre Hospitalier Universitaire Ste-Justine, University of Montreal, Montréal, Quebec H3T 1C5, Canada. [5]Institut de Recherches Cliniques de Montréal, University of Montreal, Montreal, Quebec H2W 1R7, Canada. [6]Institut National de la Santé et de la Recherche Médicale, U 968 Paris F-75012, France. [7]Department of Pharmacology and Therapeutics, McGill University, Montreal, Quebec H3A 2B4, Canada. [8]Department of Medicine, Maisonneuve-Rosemont Hospital Research Centre, University of Montreal, Montreal, Quebec H1T 2M4, Canada. [9]Department of Neurology-Neurosurgery, McGill University, Montreal, Quebec H3A 2B4, Canada.
*Corresponding author. Email: mike.sapieha@umontreal.ca (P.S.); fa.mallette@umontreal.ca (F.A.M.); js.joyal@umontreal.ca (J.-S.J.)

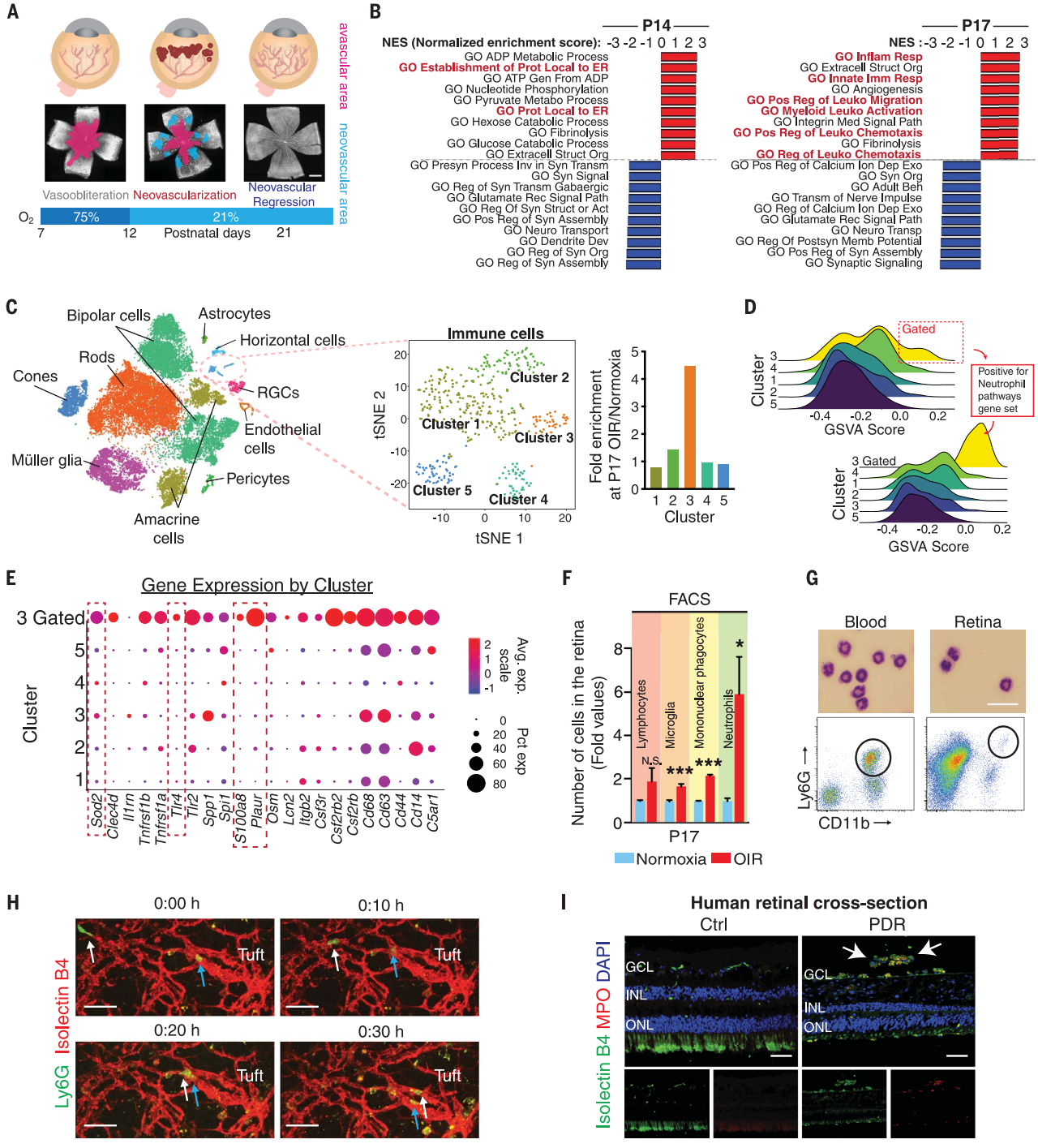

Fig. 1. Vascular remodeling in retinopathy is associated with sterile inflammation and the presence of neutrophils. (**A**) Schematic of the mouse OIR model. Exposure to hyperoxic conditions (75% O_2) in mice from P7 to P12 induces an initial phase of vascular dropout (pink). Upon return to room air at P12, ischemia triggers pathological preretinal NV that peaks at P17 (blue). From P17 to P21, preretinal NV regresses. (**B**) Hierarchal clustering of GO gene sets for RNA-seq from OIR and normoxic mouse retinas at P14 or P17 (n = 2 to 3 mice per condition). [(**C**), left inset] t-SNE for single-cell RNAseq of retinal cells from normoxic and OIR retinas at P14 and P17 (from two normoxic and three OIR sets of data) and subclustering of immune cells reveal five distinct cell populations. Each dot represents one cell. [(C), right inset] Cluster 3 displays a 4.5-fold enrichment in cells in OIR compared with normoxic controls, with positive GSVA score enrichment for genes classically found in neutrophils (**D**). (**E**) Dot plot representing expression level and frequency among cell clusters for neutrophil-related genes in each of the five populations identified in (C) as well as the neutrophil-enriched population gated from cluster 3 as performed in (D). (**F**) Accretion in OIR of lymphocytes, microglia, mononuclear phagocytes, or neutrophils assessed at P17 by FACS (see gating strategy in fig. S4) (n = 3, 6 to 9 mice/group). (**G**) The presence of neutrophils was evaluated by sorting $Ly6G^+/CD11b^+/F4/80^-$ cells from OIR retinas and staining with Giemsa (n = 5 mice). (**H**) Live-cell tracking by confocal microscopy identifies neutrophils (see arrows) migrating toward a preretinal tuft in P17 OIR retinas representative of three separate experiments. (**I**) Retinal cross sections from human patients with PDR showing invasion of MPO^+ neutrophils [(I), right inset], which are absent from control patients [(I), left inset]. Scale bars: (A), 500 μm; (G), 20 μm; (H), 50 μm; (I), 100 μm. ONL, outer nuclear layer; INL, inner nuclear layer; GCL, ganglion cell layer. For (F), *P < 0.05, *** P < 0.001, Student's t test. Data are shown as means ± SEM.

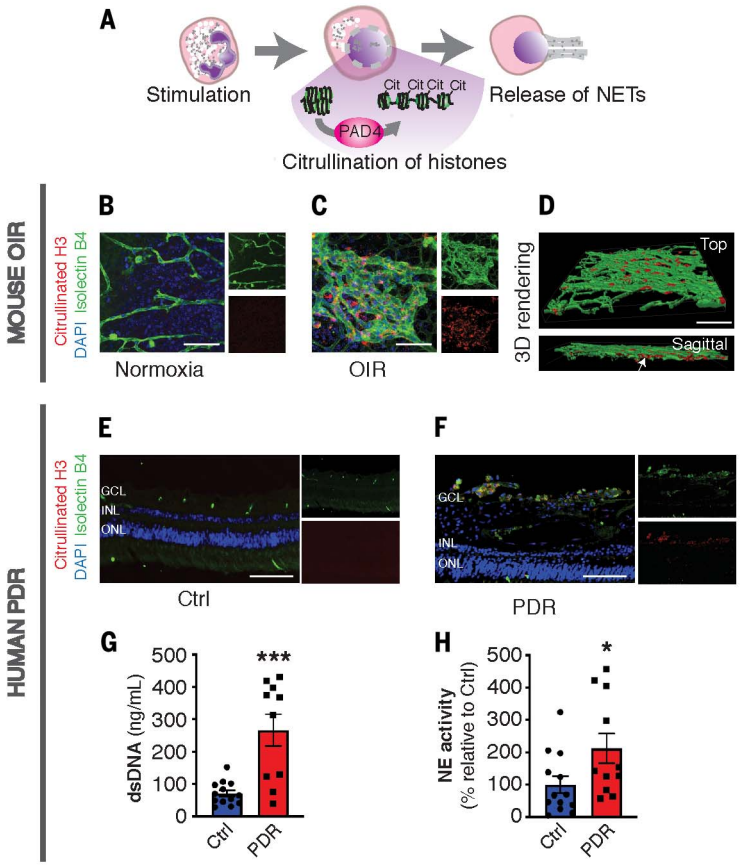

Fig. 2. NETs are found on vascular tufts. (**A**) Production of NETs is mediated by the enzymatic activity of PAD4, which citrullinates histones to allow relaxation and extracellular release of nuclear DNA. (**B** and **C**) Representative confocal micrographs of retinal flat mounts at P17 with immunofluorescence for citrullinated histone H3. NETs are absent from normoxic retinas (B) and present in retinas after OIR (C) (results are representative of three separate experiments). (**D**) Three-dimensional rendering of NETs in retinas at P17 of OIR. Immunofluorescence for citrullinated histone H3 in human retinal cross sections reveals selective staining in retinal vessels (isolectinB4-stained) of a patient with PDR compared with a patient with no known vascular pathology (**E** and **F**). dsDNA was ~3.7-fold higher (**G**) and neutrophil elastase (NE) activity was ~2.1-fold higher (**H**) in the vitreous of patients with PDR compared with controls with nonvascular pathology (n = 13 controls and 11 PDR patients; see Table 1 for patient details). *P < 0.05, ***P < 0.001, Student's t test. Scale bars: (B) to (D), 50 μm; (E) and (F), 100 μm. Data are shown as means ± SEM.

activated leukocytes contained a fraction of cells with enhanced expression of the biological pathways traditionally found in neutrophils (Fig. 1, D and E, and fig. S1C) and expressed inflammatory neutrophil–associated genes such as *Sod2*, *S100a8*, *Tlr4*, and *Plaur* (Fig. 1E).

To verify these findings, we designed specific gene sets to investigate the main effectors of the innate CNS immune response, microglia, macrophages, and neutrophils, with bulk RNA sequencing, and used curated GO gene sets specific for leukocyte functions such as migration or activation (figs. S2 and S3, respectively). Gene-set enrichment analysis (GSEA) revealed a strong positive correlation at P17 of OIR in gene clusters associated with microglia [normalized enrichment score (NES) = 2.018; false discovery rate (FDRq) = 0.000], mononuclear phagocytes (NES = 2.067; FDRq = 0.000), as well as neutrophils (NES = 2.257; FDRq = 0.000) (fig. S2), consistent with the potential presence of neutrophils at a time when regression of pathological vasculature occurs.

Neutrophils invade sites of pathological vasculature in humans and mice

Although microglia, monocytes, and mononuclear phagocytes have been well studied in retinal sterile inflammation during retinopathy (*32*–*34*), the contribution of neutrophils is ill-defined. Unlike macrophages and microglia, neutrophils are typically associated with the initial phases of inflammation. However, we observed neutrophil-related transcripts in the late stages of disease when pathological vasculature resolves. Neutrophils have relatively low transcriptional activity, so we sought to determine their presence in the retina using complementary approaches. First, fluorescence-activated cell sorting (FACS) analysis showed that neutrophils ($CD45^+/CD11b^+/Ly6C^{int}/Ly6G^{high}$) were robustly increased in the retina at P17 of OIR (~6-fold; Fig. 1F and fig. S5A; also see fig. S4 for the gating strategy). Other myeloid populations were also increased in OIR, such as mononuclear phagocytes (~2.2-fold) and microglia (~1.7-fold), but not lymphocytes (Fig. 1F). Moreover, a time-course assessment by FACS over the duration of OIR revealed that neutrophils specifically arrived at P17 when vascular regression was initiated (fig. S5B).

This population of cells was sorted and stained with Giemsa, and displayed polymorphonuclear structures characteristics of neutrophils (Fig. 1G). We then performed a myeloperoxidase (MPO) assay to detect the enzymatic activity of neutrophils. MPO is a heme-based peroxidase enzyme found at high levels in the primary granules of neutrophils (*35*). Consistent with our data, a robust increase in MPO enzymatic activity was observed at P17 of OIR compared with normoxic controls (fig. S5C). In addition, immunostaining for MPO revealed a preferential localization of neutrophils to neovascular tufts but was almost absent outside of tufts or in healthy normoxic retinas (fig. S5D). We also used ex vivo live confocal-imaging microscopy to track intraretinal neutrophils after intravenous infusion of a $Ly6G^+$ antibody. Neutrophils were found to be migrating toward neovascular tufts in retinas from pups at P17 of OIR (Fig. 1H and movie S1). Finally, immunostaining of cross sections of eyes from human patients with PDR using an antibody raised against MPO detected neutrophils in the proximity of neovascular tufts, confirming their presence in human pathology (Fig. 1I).

NETs are released on pathological retinal vasculature in humans and mice

Given the potential role of neutrophils in sterile inflammation (*36*), as well as their presence at the onset of vascular remodeling (Fig. 1), we investigated how these cells influence vascular remodeling. One of the potential features of neutrophils is their ability to exude extracellular traps. Neutrophil extracellular traps (NETs) are primarily described as being deployed to sequester against invading bacteria and fungi through a mesh of DNA decorated with granular proteins (MPO, elastase, and cathelicidin) (*37*). The extrusion of NETs is dependent on the citrullination of histones by the peptidyl arginine deiminase type IV (PAD4) enzyme and decondensation of the chromatin (*38*) (Fig. 2A). In addition to their bactericidal properties, NETs have also been documented in sterile inflammation in cases of atherosclerosis (*39*) or ischemia-reperfusion injury (*40*). We therefore sought

Table 1. Clinical characteristics of patients who underwent vitreous biopsy.

Pathology	Sex	Age*	Diabetes	
			Type	Duration (y)
Control patients				
MH	M	71	-	-
MH	F	76	-	-
MH	F	74	-	-
ERM	F	46	-	-
ERM	F	84	-	-
ERM	F	77	-	-
ERM	M	57	-	-
MH	M	82	-	-
MH	M	65	-	-
ERM	F	69	-	-
ERM	M	69	-	-
ERM	M	81	-	-
MH	F	65	-	-
Diabetic patients				
PDR	F	56	NA	NA
PDR	M	80	NA	28
PDR	M	74	II	NA
PDR	F	72	NA	NA
PDR	M	35	NA	NA
PDR	M	36	II	NA
PDR	F	70	II	40
PDR	F	74	NA	35
PDR	F	67	II	30
PDR	M	69	II	4
PDR	M	45	II	NA

MH, macular hole; ERM, epiretinal membrane; NA, not available *Mean age for control patients, 70.5 ± 2.9 years; mean age for diabetic patients, 61.6 ± 4.8 years.

to determine whether NETs were found in retinas during the phases of vascular remodeling when neutrophil levels are elevated. We performed immunofluorescence against citrullinated histone H3 on retinas from mice at P17 of OIR and detected NETs adjacent to pathological neovascular tufts (Fig. 2, B to D), but they were absent from normoxic controls. These structures colocalized with MPO, a neutrophil marker and a constituent of NETs (fig. S6, A and B).

Next, we sought to determine whether our findings in mice held in humans with pathological retinal vasculature. We investigated the presence of NETs in patients with PDR. Immunofluorescence on retinal cross sections from control patients with no identified vascular pathology did not show any evidence of citrullinated histone H3 (Fig. 2E). Conversely, citrullinated histone H3 was detected in preretinal ECs (isolectin B4-stained) of individuals with PDR (Fig. 2F). Patients with PDR showed protrusion of vessels at the vitreoretinal interface characteristic of preretinal NV as determined by spectral domain optical coherence tomography (fig. S6C, white arrow). To further verify the presence of NETs in diabetic patient retinas, we analyzed the vitreous humor from patients with PDR for the presence of double-stranded DNA (dsDNA) that could be released secondary to NET production. Concentrations of dsDNA in the vitreous humor of patients with PDR were significantly higher compared with controls with nonvascular pathology such as idiopathic epiretinal membrane or macular hole (Fig. 2G). Moreover, we also detected significantly higher levels of elastase activity (associated with NET production) (*41*) in the vitreous humor of patients with PDR (see Table 1 for patient characteristics and Fig. 2H). Thus, NETs are associated with retinal vascular disease in mice and humans and are found at sites of pathological angiogenesis.

Neuronal and vascular units have distinct patterns of cellular senescence and secretory phenotypes in OIR

We next sought to elucidate the stimulus for NETosis in pathological retinal vasculature. ECs in preretinal NV as well as retinal ganglion cell (RGCs) undergo cellular senescence in OIR (*11*). Using GSVA on single-cell transcriptomic data for gene sets related to cellular senescence and two gene sets related to secretory processes, we found that neurons such as RGCs were senescent but did not readily display a classical transcriptional signature of the senescence-associated secretory phenotype (SASP) and did not transcribe genes related to cytokine secretion (Fig. 3A). By contrast, ECs (green box), pericytes, astrocytes, Müller glia, and immune cells up-regulated transcripts were related to cellular senescence and triggered a SASP (Fig. 3A).

SASP expression plotted on t-SNE from retinal populations at P17 of OIR (Fig. 3, B and C), as well as hierarchical comparison of genes for the SASP (Fig. 3D), showed that astrocytes, ECs, Müller glia, and pericytes adopted a robust SASP transcriptional signature. Thus, whereas several cell populations of the retina undergo cellular senescence in retinopathy, non-neuronal and neuronal populations adopt different secretory transcriptional signatures.

Senescent vascular endothelium triggers the release of NETs

NETs (visualized with extracellular citrullinated H3) were regularly found adjacent to senescent isolectin-positive ECs [stained for promyelocytic leukemia (PML) protein, a key regulator of cellular senescence (*42*, *43*)] (Fig. 4A and fig. S7A), as well as in $NG2^+$ pericytes (fig. S7B), but not in Müller cells or astrocytes [both positive for glial fibrillary acidic protein (GFAP); fig. S7C]. Thus, because several known factors of the SASP overlap with reported inducers of NETs (fig. S8), we investigated whether NETs could be triggered by senescent vascular ECs.

Classical triggers of cellular senescence include DNA damage, telomere attrition, mitochondrial dysfunction, and oncogene activation as in oncogene-induced senescence (*44*). The latter can be induced by various oncogenes, including sustained activation of the GTPase RAS (*45*), which triggered senescence through the DNA damage response and activation of p53 (*46*–*48*). We observed robust activation of the RAS pathways within preretinal pathological angiogenic sprouts either by immunostaining for phospho-ERK1/2 (a kinase downstream of RAS) (Fig. 4B and fig. S9A) or GSVA of single-cell transcriptomics (Fig. 4C). The bimodal enrichment for KRAS-associated pathways in ECs (Fig. 4C) suggested a distinct population of cells, with those in neovascular tufts likely showing higher activation (right peak) and less proliferative ECs showing lower activation (left peak). Indeed, these high-RAS ECs (red square) were not found in normoxic control retinas (fig. S9B), which suggested that senescent cells might coincide with neovascular tufts. Normoxic control retinas also showed inferior levels of RAS activation compared with those in OIR. To investigate which subsets of cells interacted with $KRAS^+$ cells in retinopathy, we performed CellPhoneDB analysis, a bioinformatics tool that

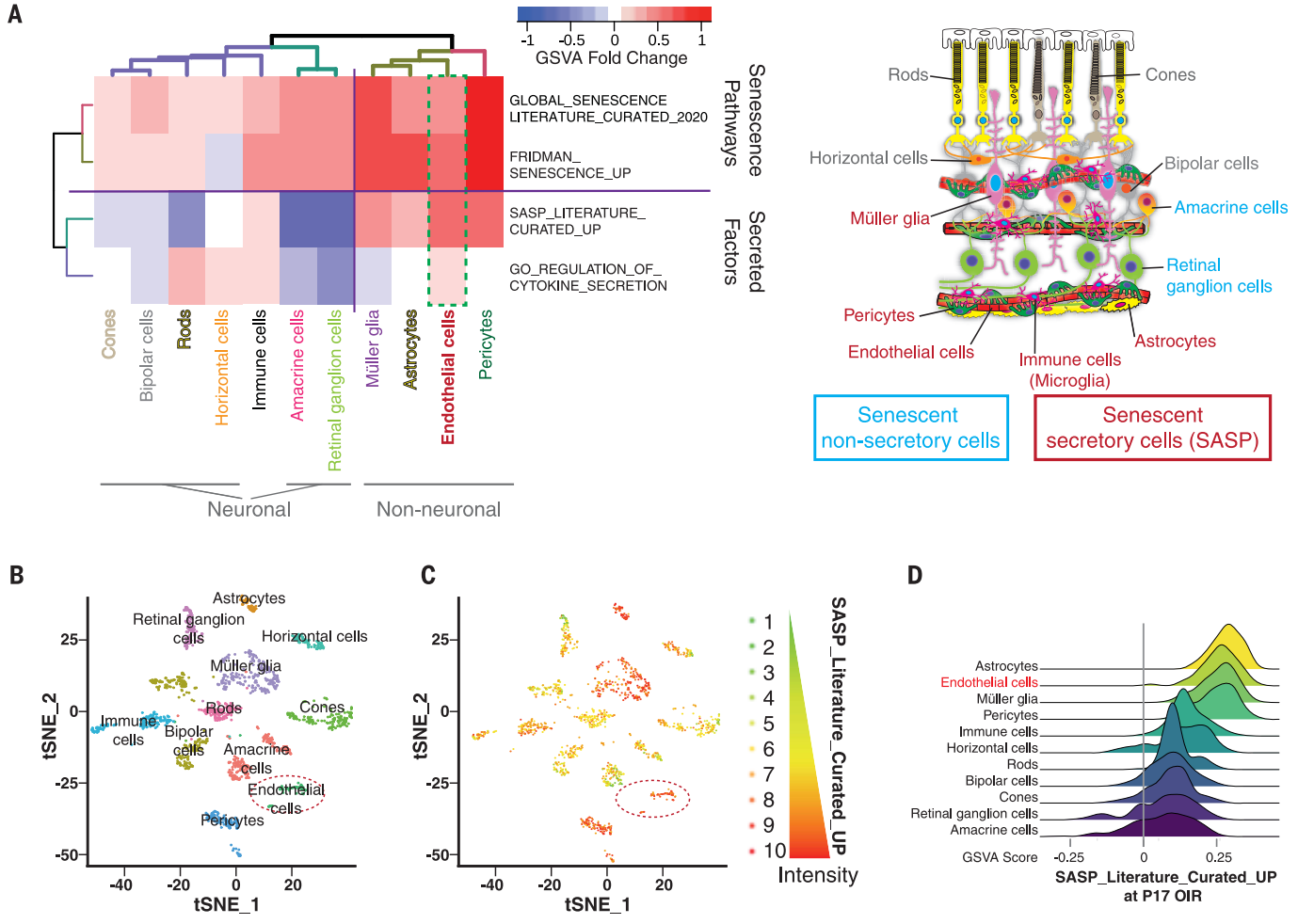

Fig. 3. Neurons and mitotic cells display distinct gene signatures of cellular senescence in retinopathy. (**A**) Fold change of GSVA score on gene sets related to cellular senescence and cytokine secretion comparing transcripts from scRNAseq of P17 normoxic and OIR retinas. (**B** and **C**) t-SNE and (**D**) hierarchical clustering of cell populations from P17 retinas ranked by absolute GSVA score reveals that in OIR, astrocytes, ECs, Müller glia, and pericytes induce a SASP response compared with other cell types. Data presented were downsized to display a maximum of 1000 cells per retinal cell type.

builds cell-cell communication networks using ligand-receptor information from available single-cell transcriptomic data (*49*). We observed increased interactions between cluster 3 (shown to contain neutrophils; Fig. 1, C and E) and KRAS^{+} ECs (Fig. 4D). Lower numbers of interactions were found with nonsenescent ECs. These data support the idea that neutrophils interact with senescent ECs in retinopathy.

RAS activity is elevated in active preretinal NV (*50*), and the expression of γH2AX and PML (key modulators of RAS-induced senescence) is observed in pathological ECs during retinopathy (*11*). To explore the mechanism by which senescent ECs trigger NETs, we generated a model of cellular senescence in human umbilical vein endothelial vascular cells (HUVECs) by sustained activation of the RAS pathway. Activation of RASV12 leads to a strong mitogenic signal driven by the Raf-MEK-ERK pathway, leading to a DNA damage checkpoint response, cell cycle arrest, and then senescence (*46*, *47*). RASV12 activation was verified (fig. S10, A to C) and induction of cellular senescence in ECs confirmed using senescence-associated β-galactosidase staining (SA-β-Gal) 10 days after infection (67 ± 10% for RASV12-infected cells versus 3 ± 3% for the empty vector) (fig. S10D).

To determine whether senescent ECs were able to provoke the release of NETs, we seeded senescent as well as proliferating ECs into multiwell chambers and then introduced freshly isolated human blood neutrophils colored by DiI Red to EC cultures the following day and stained with a dye labeling extracellular DNA (SYTOX Green). Time-lapse imaging revealed a modest release of extracellular DNA from neutrophils incubated with control ECs (empty vector) (Fig. 4, E and F). By contrast, neutrophils discharged loads of DNA in the presence of senescent ECs (Fig. 4, E and F). Conditioned media from RAS-overexpressing senescent ECs was sufficient to trigger NET release, suggesting that a soluble factor secreted during cellular senescence was mediating NET release (Fig. 4E).

To identify factors produced by senescent cells that trigger NETosis, we performed SILAC (stable isotope labeling using amino acids in cell culture). Senescent or proliferating HUVECs were labeled with either light or heavy arginine and lysine 13C6 and 15N2 (fig. S11A). Secreted proteins released from empty vector–transduced cells were mixed in equal proportion to those from RASV12-infected HUVECs. The relative abundance of identified peptides was calculated after mass spectroscopy (MS)/MS analysis and MaxQuant postanalysis. We clustered the proteomic data using the Reactome database (*51*) and found that the secretome of senescent ECs was primarily enriched in proteins related to immune pathways (Fig. 4G), including proteins involved in cytokine signaling (Fig. 4H). These SILAC data were corroborated by the secretome of IMR90 senescent

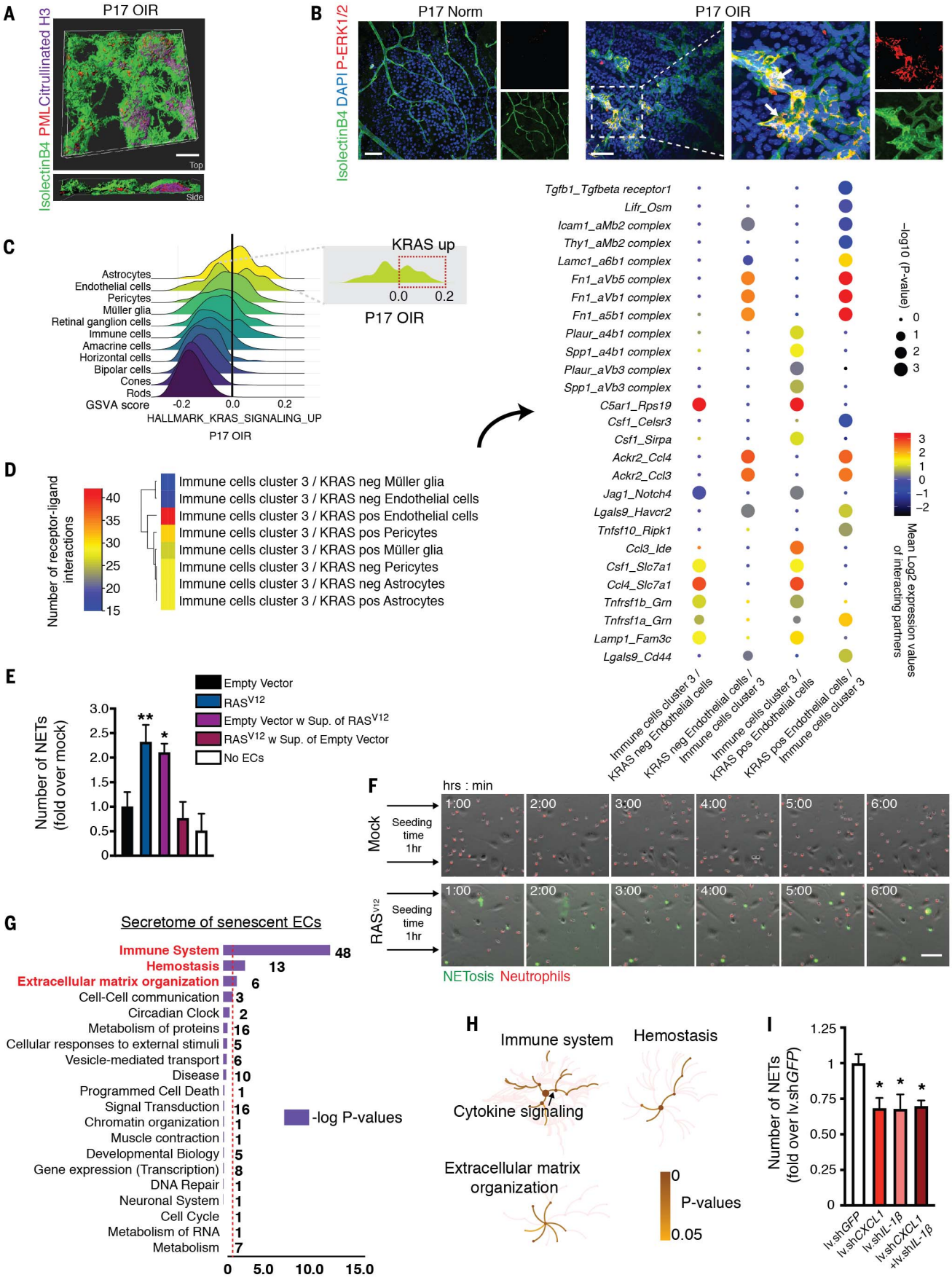

Fig. 4. Senescent ECs trigger NETosis. (**A**) Representative confocal micrograph and three-dimensional reconstruction of PML and citrullinated histone H3 at P17 of OIR. PML is mainly expressed on retinal tufts and often colocalizes with NETs (citrullinated histone H3 staining) (n = 3 separate experiments). (**B**) Increased phosphorylation of ERK1/2 is observed by immunofluorescence in P17 OIR retinas compared with normoxic controls. Results shown are representative of three experiments. (**C**) Ridge plots of GSVA score for KRAS-associated transcriptional signatures of single-cell RNAseq of retinas at P17 OIR reveal enrichment primarily in astrocytes, ECs, and pericytes. Inset, ECs display bimodal distribution for KRAS-associated gene set expression. (**D**) CellPhoneDB analysis predicts increased interaction between immune cells of cluster 3 and $KRAS^+$ ECs gated on GSVA score [see inset in (C)]. Data are expressed as the total number of ligand-receptor interactions between immune cell cluster 3 and KRAS gated retinal cell type (see heatmap in left inset). These interactions are displayed for ECs and immune cell cluster 3 in an array of ligand-receptor couples (see dot plot in right inset), with dot color and size representing the strength and significance of the predicted interaction between cell types. (**E**) Quantification of NETs in (**F**) shows a >2-fold induction of NETosis with RAS^{V12}-transduced cells or empty vector–infected cells with supernatant from RAS^{V12}-infected cells (empty vector w Sup. of RAS^{V12}) compared with empty vector–infected cells (n = 3 experiments). (**F**) Representative time course of human neutrophils stained with Dil Red and coincubated with RAS^{V12}-expressing HUVECs. NETosis was visualized with SYTOX Green (n = 3 experiments). (**G**) SILAC-based MS-MS analysis of proteins up-regulated at least 1.5-fold and analyzed through the Reactome database shows primary enrichment in peptides related to immune system regulation in RAS^{V12}-infected senescent ECs compared with mock-infected controls. Numbers in adjacent bars represent the quantity of connections found. Top three nodes (bold) have an FDR < 0.05 (from two independent sets of labeled proteins). (**H**) Overrepresentation analysis showing pseudocolored nodes according to their P values. Cytokine signaling pathways are enriched in proteins from senescent RAS^{V12}-infected ECs (black arrow). Darker colors represent nodes with lower P values (higher activation). (**I**) Targeted depletion of *CXCL1*, *IL-1*β, or both by Lv.shRNAs in RAS^{V12}-transduced senescent ECs significantly decreases NETosis (n = 3 separate experiments). Scale bars: (A) and (B), 50 μm; (F), 20 μm. For (E) and (I), one-way ANOVA with Bonferroni's test was used (*P < 0.05, **P < 0.01). Data are shown as means ± SEM.

fibroblasts (*52*), which shared the same top three enrichment clusters of immune regulation, hemostasis, and extracellular matrix reorganization (fig. S11B). On the basis of enrichment in cytokine signaling, we confirmed by real-time quantitative polymerase chain reaction (PCR) increased transcription of cytokines such as interleukin 1β (IL-1β) or CXCL1 in RASV12-infected HUVECs (fig. S12A). To determine whether these cytokines contribute to NETosis, we generated HUVECs depleted for IL-1β, CXCL1, or both cytokines through lentiviral transduction of short hairpin RNAs (shRNAs) (fig. S12, B and C). Down-regulation of either IL-1β or CXCL1 in senescent cells led to a significant reduction in NETosis (Fig. 4I). Combined knock-down of IL-1β and CXCL1 did not further reduced NETosis, suggesting potential redundancy (Fig. 4I). Therefore, senescent ECs release cytokines as part of their SASP (*53*), which prompts neutrophils to release NETs.

NETs remodel retinal vasculature through apoptotic elimination of senescent ECs

Typically, cellular senescence and apoptosis are mutually exclusive cell fates. However, NETs can be cytotoxic for ECs (*54*, *55*). In OIR retinas undergoing pruning of pathological vasculature, we noted higher numbers of apoptotic ECs ($IB4^+$ cells; Fig. 5A). Apoptotic ECs were confined to areas of pathological NV (tufts) and absent from areas outside tufts or normoxic control retinas (Fig. 5A and fig. S13). Given that senescent pathological neovasculature regresses after P17 in mouse OIR, we investigated whether NETs projected onto pathological neovasculature could influence clearance of senescent ECs ($IB4^+$ cells) in OIR. We injected DNase I into the vitreous humor of mice at P17 of OIR to promote degradation of NETs (as confirmed by immunohistological staining; fig. S14) and then analyzed the area of retinal SA-β-Gal activity at P19. Injections of DNAse I stalled the clearance of senescent cells, as seen by an enhanced proportion of SA-β-Gal^+ area in the retina at P19 of OIR (Fig. 5B). Correspondingly, DNAse I treatment resulted in persistence of the senescence-associated genes *Pai1 (Serpine1)* and *IL-1*β in the retina (Fig. 5C). To investigate the role of PAD4, an essential enzyme for NETosis (*56*), we generated a Pad4-deficient mouse within the myeloid compartment by crossing mice expressing the Cre enzyme under the LysM promoter with mice harboring loxP sites flanking the *Pad4* gene (fig. S15A). LysM was expressed by >95% of neutrophils, as confirmed by FACS analysis (fig. S15B). Efficient diminution of PAD4 levels in LysM-$cre^{+/+}$*Pad4*$^{-/-}$ mice was confirmed by immunoblot on mouse blood neutrophils (fig. S15C). Impeding NETosis through genetic ablation of myeloid-resident Pad4 resulted in a persistence of senescent ECs at P19 of OIR, as determined by senescence-associated markers such as PML in retinal tufts (Fig. 5D). Exposing RASV12-infected senescent ECs to NETs isolated from activated neutrophils resulted in a dose-dependent cleavage of caspase-3, suggesting that NETs could trigger apoptosis of senescent ECs (Fig. 5E). EC apoptosis upon exposure to NETs was confirmed by annexin V staining (Fig. 5F).

NETs participate in clearing pathological retinal vasculature

Finally, we investigated the consequences of abrogating NETosis on NV in ischemic retinopathies. First, we injected DNase I into the vitreous humor of mice subjected to OIR with the aim of degrading NETs (*57*) either during (P15) or after (P17) vascular tuft formation. We also used a complementary approach involving a neutrophil-depleting antibody (anti-Ly6G) (*58*), which abrogated neutrophils in both blood and retinas of mice without affecting other leukocyte populations (see assessment by FACS shown in fig. S16, A and B). The status of the retinal vasculature was assessed 2 days after injection for the extent of pathological preretinal angiogenesis (neovascular area) and the extent of vascular regeneration (avascular area). These two parameters can be interdependent, with regression of neovascularization influencing the rate of revascularization (*59*). Treatment with either DNase I or anti-Ly6G during the phase of vascular proliferation at P12 or P15 did not influence NV (fig. S17, A and C), nor did it stimulate revascularization of avascular zones of the retina (fig. S17, B and D), compared with vehicle or isotype controls. By contrast, when DNase I or anti-Ly6G were injected at P17 of OIR during peak NV, pathological NV persisted (Fig. 6A) and vascular regeneration was impeded as assessed at P19 (Fig. 6B). Thus, various approaches to prevent NETosis in OIR by either depleting neutrophils or enzymatic removal of NETs with DNase I stalled regression of pathological vessels and consequently prevented the regeneration of functional blood vessels into the ischemic retina.

To corroborate these findings, we used cre-$LysM^{+/+}$*Pad4*$^{-/-}$ mice. As described above, we evaluated the propensity of these mice to clear pathological NV and influence vascular regeneration in OIR. The absence of myeloid-resident PAD4 did not influence the onset or development of preretinal NV (Fig. 6C), nor did it affect vascular regeneration as assessed at P17 of OIR (Fig. 6D). However, as with the interventional approaches described above (Fig. 6, A and B), deficiency in myeloid-resident PAD4 compromised the regression of pathological preretinal blood vessels (Fig. 6E) while consequently preventing regrowth of functional vessels (Fig. 6F) as determined at P19 OIR. Similarly, inhibition of either IL-1β signaling with IL-1 receptor antagonist (Kineret) or CXCL1 signaling with the CXCR2 inhibitor SB265610 at the time of maximal NV (P17) reduced remodeling of pathological vasculature as determined at P19, further supporting the importance of inflammatory cytokines in mediating the clearance of pathological neovasculature (fig. S18, A to D). Inhibition of IL-1β before NV (P15) prevented pathological

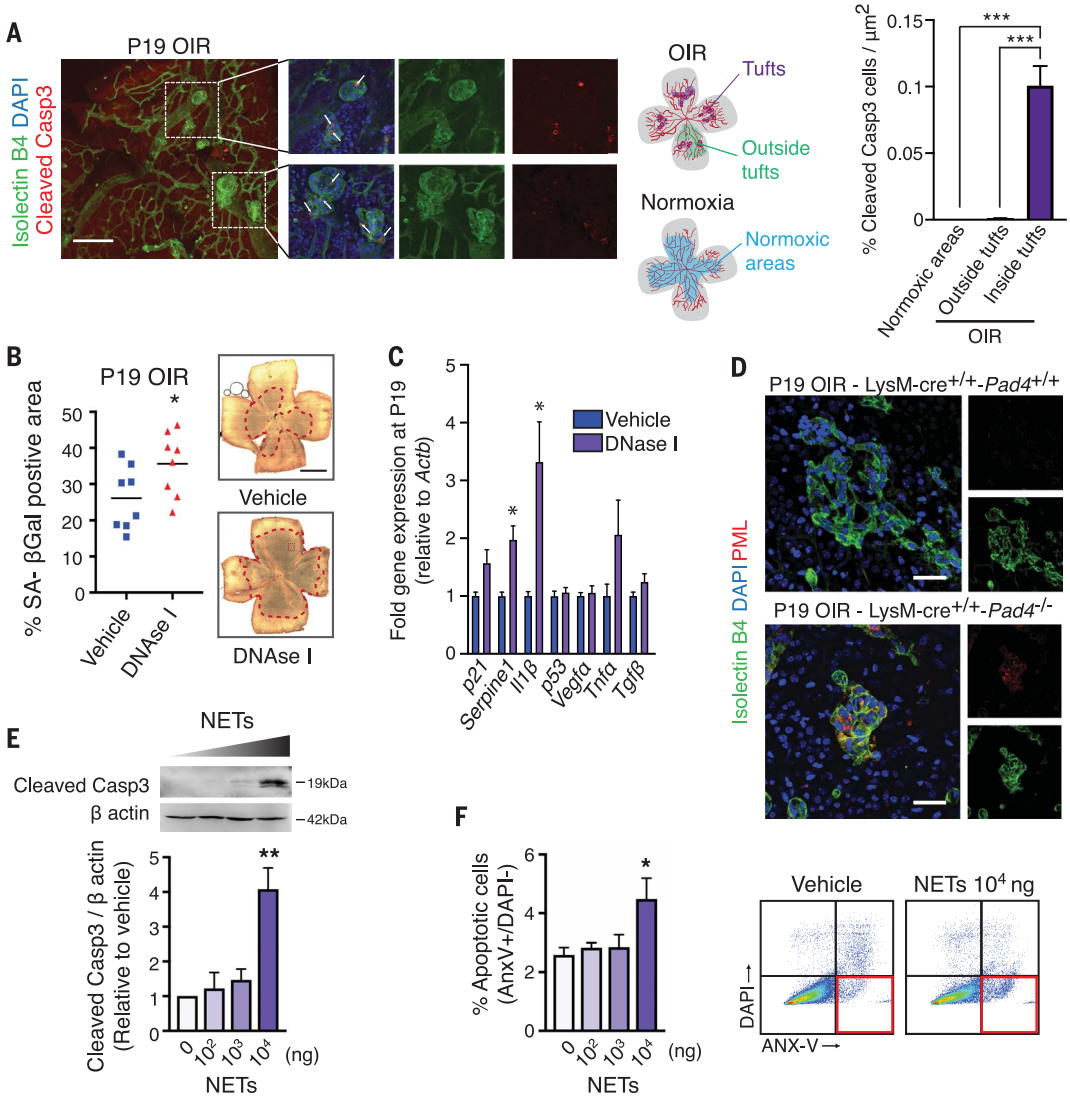

Fig. 5. NETs clear senescent ECs by inducing apoptosis. (**A**) (Left inset) Cleaved caspase-3$^+$ apoptotic cells (white arrows) are found in P19 OIR flat mounts and colocalize with isolectin-B4$^+$ ECs almost exclusively in neovascular tuft areas (right inset) ($n \geq 3$ separate experiments). (**B**) Intravitreal injection of DNAse I at P17 of OIR results in persistence of SA-β-Gal$^+$ senescent cells and (**C**) mRNA transcripts for certain SASP factors at P19 (both $n = 3$ separate experiments). (**D**) PML$^+$ senescent cells persist in LysM-cre$^{+/+}$*Pad4*$^{-/-}$ retinas at P19 of OIR as opposed to LysM-cre$^{+/+}$*Pad4*$^{+/+}$ controls (results shown are representative of three separate experiments). (**E**) (Top) Immunoblots showing a dose-dependent induction of active cleaved caspase-3 protein in RAS^{V12}-infected senescent HUVECs upon incubation with escalating doses of NETs with a sharp rise with 10^4 ng. (Bottom) Densitometric analysis of caspase-3 protein expression reveals an ~4-fold induction of cleaved caspase-3 expression with 10^4 ng of NETs ($n = 3$ independent experiments). (**F**) Incubation of RAS^{V12}-infected senescent HUVECs with 10^4 ng of NETs provokes 1.7-fold more apoptosis as assessed by annexin V surface staining ($n = 4$ different experiments). For (B) and (C), Student's *t* test was used (*$P < 0.05$); for (E) and (F), one-way ANOVA with Bonferroni's test was used (*$P < 0.05$, **$P < 0.01$). Scale bars: (A) and (D), 200 µm; (B), 1 mm. Data are shown as means ± SEM.

angiogenesis (fig. S18, E and F), as expected (*60*, *61*). Therefore, neutrophils, through the release of NETs, target pathological senescent ECs for clearance and prepare the ischemic retina for reparative vascular regeneration.

Discussion

Complex tissues of the central nervous system, consisting predominantly of postmitotic cells such as the retina and the brain, require an inherent ability to rapidly adjust to environmental stressors or to rapidly remodel after injury. Here, we tested two concepts pertaining to vascular remodeling in ischemic retinopathies. First, we investigated the idea that neutrophils, which are classically associated with a first wave of invading leukocytes, are also involved in late stages of the sterile inflammatory response during retinal vascular remodeling. Second, we investigated whether neutrophils responding to the secretome of senescent ECs and likely other cells of the vascular unit and through extrusion of NETs eliminate diseased vasculature by triggering its apoptosis. Clearance of pathological blood vessels is a key step for tissue repair and resolution of inflammation in ischemic retinopathies and enables tissue remodeling. Conceptually, the selective removal of ECs that have engaged pathways shared with aging and cellular damage suggests an origin for programs of cellular senescence in ensuring tissue fitness. Diseased cells discharge a SASP, favoring their clearance and later restoration of functional vascular networks. Postmitotic neurons such as RGCs, which undergo postmitotic cellular senescence during OIR (*62*), do not readily engage a classical SASP transcriptional gene signature, suggesting that they would evade targeting by immune cells.

Cellular senescence is a dynamic response to various stressors including oxidative damage, telomere attrition, ischemia, metabolic imbalances, activated oncogenes, and chemotherapy (*62*, *63*). Pathways that lead to cellular senescence are potent tumor-suppressive mechanisms and limit the division and spread of premalignant cells (*64*). Moreover, in response to the secretion of immunomodulatory factors of the SASP (*52*), senescent cells prime neighboring cells for reprogramming (*65*–*67*) while allowing for clearance of malignant cells as part of an intrinsic program to stall tumor development and fibrosis (*68*–*70*). Collectively, these mechanisms set the stage for tissue repair and remodeling (*63*, *66*, *67*) and are consistent with the processes engaged to clear pathological vasculature in the retina (*71*, *72*).

To date, the removal of senescent cells by the immune system has been ascribed to natural killer (NK) cells, which use the NK2GD receptor (*68*–*70*, *73*) and macrophages during, for example, salamander limb regeneration (*74*)

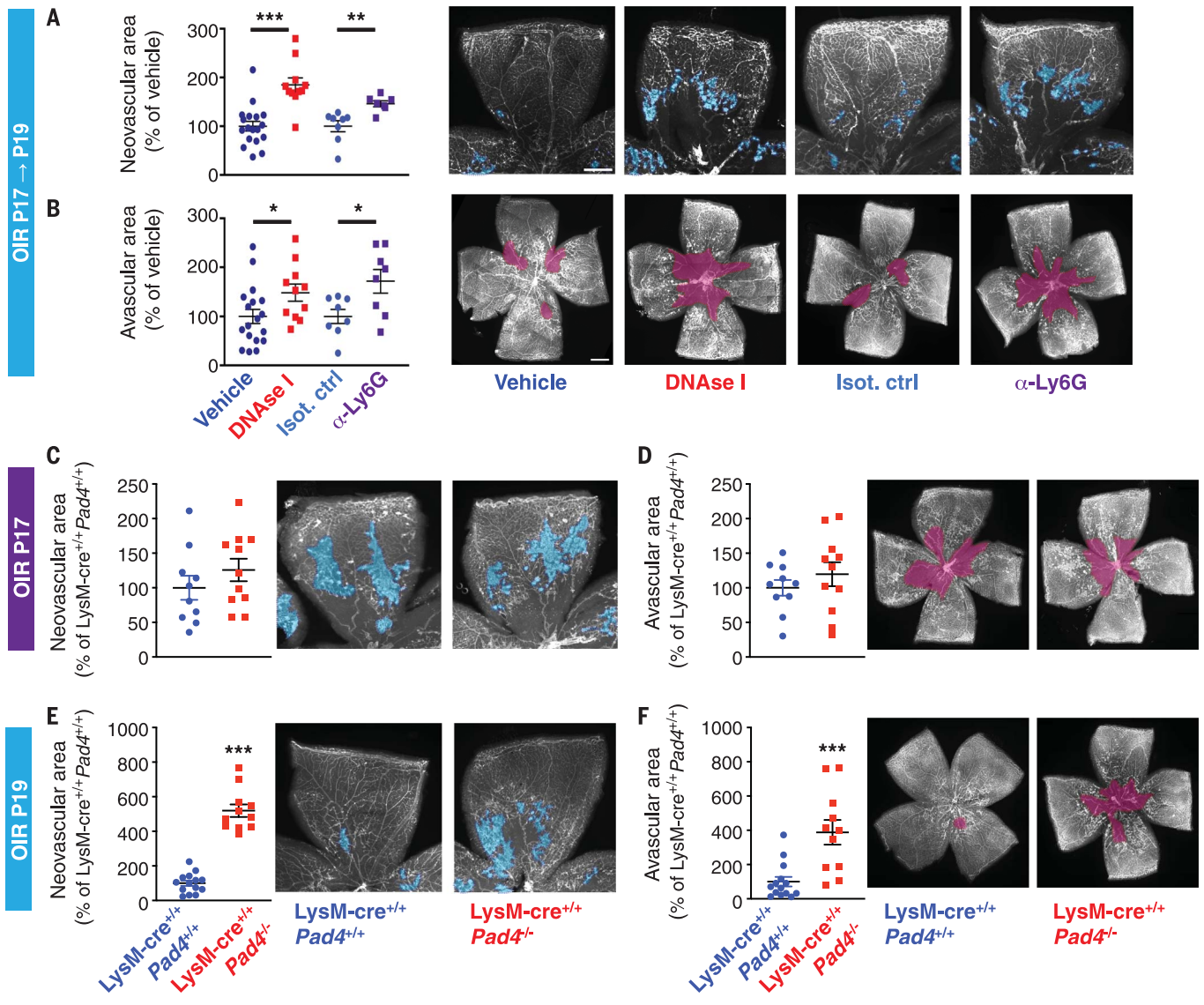

Fig. 6. NETs promote the regression of pathological vasculature in retinopathy. (**A**) Injections of DNAse I or anti-Ly6G at P17 of OIR prevented regression of preretinal NV, leaving ~1.8-fold higher NV with DNAse I and ~1.5-fold higher NV with anti-Ly6G at P19. (**B**) A similar decrease in vascular regeneration was observed with ~1.5-fold higher avascular areas with DNAse I and ~1.7-fold higher avascular areas with anti-Ly6G (n = 8-18 retinas). (**C**) LysM-cre$^{+/+}$*Pad4*$^{-/-}$ and LysM-cre$^{+/+}$*Pad4*$^{+/+}$ mice developed similar amounts of preretinal NV and showed similar rates of vascular regeneration (**D**) at P17 of OIR, but LysM-cre$^{+/+}$*Pad4*$^{-/-}$ mice showed retarded clearance of these vascular tufts at P19 (5.2-fold higher NV) (**E**) and ~3.7-fold larger avascular areas (**F**) (n = 10-14 retinas) Scale bars, 0.5 mm. Data were analyzed with Student's t test (*P < 0.05, **P < 0.01, *** P < 0.001) and are shown as means ± SEM.

and the clearance of senescent hepatocytes in hepatocarcinoma (*68*). Induction of cellular senescence in hepatic carcinomas through reactivation of p53 promotes tumor regression through the elimination of senescent tumor cells by the innate immune system, and it has been suggested that NK cells, macrophages, and neutrophils contribute to similar degrees through an unexplored mechanism (*70*). Our findings suggest that prolonged exposure of senescent ECs to NETs directly triggers a cytotoxic response leading to apoptotic death. This likely occurs from direct exposure to protein constituents such as histones or MPO (*54*). Ultimately, neutrophil-mediated NETosis might facilitate further clearance through innate immune phagocytosis.

Quantitative proteomics using SILAC revealed that senescent ECs predominantly induce a secretome involved in immune regulation. Subsets of ECs in retinopathy adopt a SASP and excrete cytokines such as CXCL1, IL-1β, and others, similar to what has been described for other senescent cell populations (*53*). Inhibition of these cytokines or their receptors curtails senescence-induced NETosis and impedes neovascular tuft regression, highlighting the role of these inflammatory factors in vascular remodeling. We cannot exclude that other mediators of the SASP response, such as reactive oxygen species, might contribute to NETosis. In addition to ECs, vascular-associated cells such as pericytes and Müller glia also trigger a SASP.

Although removal of diseased senescent vasculature through a neutrophil-mediated process may be an intrinsic reparative mechanism that favors tissue remodeling after vascular lesions, uncontrolled retinal neutrophila and abundant NETosis in the retina may be incompatible with proper retinal health. Retinal NETosis may potentially exacerbate retinal

vasculopathy by causing microvascular occlusions or small-vessel vasculitis secondary to the development of autoantibodies against the neutrophil elastase and MPO found in NETs (*75*). This is corroborated by retinal microvascular preservation in diabetes after immunodepletion of neutrophils (*76*, *77*). Elevated systemic neutrophil counts are associated with DR (*78*), and elevated levels of plasma neutrophil gelatinase-associated lipocalin (NGAL) positively correlate with DR in patients with type 2 diabetes (*79*). Further potential detrimental effects for retinal NETs in DR are suggested by findings that neutrophils are associated with capillary closure in retinas from spontaneously diabetic monkeys (*80*), and circulating DNA-histone complexes and polymorphonuclear neutrophil elastase have been reported to be significantly increased in patients with DR (*81*). NETs are capable of forming elaborate networks of fibers that trap erythrocytes and platelets and provoke vascular occlusion, with a few hundred neutrophils capable of provoking millimeter-sized cloths (*82*).

By triggering age-independent pathways of cellular senescence, pathological neovasculature prompts its turnover by triggering an innate immune response. These findings suggest an etiology for cellular senescence in tissue remodeling and highlight that elimination of senescent vascular cells ameliorates the outcome of neovascular retinal disease. More broadly, our findings identify an inherent mechanism whereby bouts of sterile inflammation can remodel diseased blood vessels.

MATERIALS AND METHODS

See table S2 for a detailed description of all reagents.

Animals

All studies were performed according to the Association for Research in Vision and Ophthalmology (ARVO) Statement for the Use of Animals in Ophthalmic and Vision Research and were approved by the Animal Care Committee of the University of Montreal in agreement with the guidelines established by the Canadian Council on Animal Care. C57BL/6 wild-type mice were purchased from The Jackson Laboratory and CD1 nursing mothers from Charles River Laboratories.

Human samples and vitrectomy

Patients with PDR and controls (macular hole or epiretinal membrane) were followed and operated on by a single surgeon (F.A.R.). The study protocol followed the Declaration of Helsinki tenets and the institutional human clinical protocol. Informed consent was obtained from Maisonneuve-Rosemont Hospital (HMR) ethics committee (CER 13082). Human eye sections were obtained from the Human Eye Biobank (Toronto, Ontario).

OIR and depletion of neutrophils

Mouse pups (C57BL/6, The Jackson Laboratory) and their fostering mothers (CD1 from Charles River Laboratories or S129 from The Jackson Laboratory) were exposed to 75% O_2 from P7 to P12 and then returned to room air. Upon return to room air, hypoxia-driven NV developed from P14 on (*28*). Eyes were enucleated at different time points and the retinas dissected for mRNA. Dissected retinas were flat-mounted and incubated overnight with fluoresceinated isolectin B4 (1:100) in 1 mM $CaCl_2$ to determine the extent of the avascular area or the NV area at P17. Analysis was performed using ImageJ and the SWIFT-NV method (*83*). Avascular areas were calculated by dividing the central capillary-free area by the total retinal area. The percentage of NV was calculated by dividing the area of neovascular tufts (saturated lectin–stained vasculature on the surface of the retina) by the total area of the retina. Neutrophils were depleted from the circulation by intraperitoneal injection of the neutrophil-specific antibody Ly6G (30 mg/kg) or a rat IgG2A isotype control antibody (30 mg/kg). Depletion efficiency was assessed after FACS analysis. Intravitreal injections (1 μl) of DNAse I (10 U/μl), SB265610 (1 μm), or Kineret (150 mg/ml) were performed using a Hamilton syringe fitted with a glass capillary.

RNA sequencing and GSEA

Preparation and analysis of total RNA from OIR and normoxic retinas were as previously described (*11*). Briefly, RNA was isolated using the Dynabeads mRNA Direct Micro Kit (Thermo Fisher Scientific), and whole transcriptome analysis was done with Ion Total RNA-Seq Kit version 2. Sequencing was performed on an Ion Proton Instrument (Ion Torrent, Thermo Fisher Scientific). RNA-sequencing (RNA-seq) analysis was done using the Torrent Suite software version 5.4.0 and the RNASeqAnalysis plugin (Thermo Fisher Scientific) on the mouse reference genome mm10. GSEA was performed (www.gsea-msigdb.org/gsea/index.jsp) on pre-ranked lists based on shrunken log2-fold changes.

Drop-seq

Following the same digestion procedure described by Macosko *et al.* (*30*), single-cell suspensions were prepared from P14 and P17 normoxic and OIR C57BL/6 mouse retinas through successive steps (digestion using papain solution, trituration, and filtration) to obtain a final concentration of 120 cells/μL. The final cell suspension was obtained from either whole or rod-depleted retinas using a CD73 magnetic column (*84*). Droplet generation and cDNA libraries were performed as described in the Drop-seq procedure (http://mccarrolllab.org/dropseq/), and sequencing was carried out on an Illumina NextSeq 500 at an estimated read depth/cell similar to that used by Macosko *et al.* (*30*) (i.e., 50,000 reads/cell). Unique molecular identifier (UMI) counts from the single-cell RNA sequencing (scRNAseq) replicates of normoxic and OIR retina were merged into one single digital gene expression (DGE) matrix and processed using the "Seurat" package [spatial reconstruction of single-cell gene expression data (*85*)]. Cells expressing fewer than 100 genes and more than 10% of mitochondrial genes were filtered out. Single-cell transcriptomes were normalized by dividing by the total number of UMIs per cell and then multiplying by 10,000. All calculations and data were then performed in log space [i.e., ln(transcripts per 10,000 + 1)].

After the whole and rod-depleted dataset were aligned using canonical correlation analysis on the most variable genes in the DGE matrix (*86*), the 20 most significant components were used as input for t-SNE. To identify putative cell types on the t-SNE map, a density-clustering approach was used and average gene expression was computed for each of the identified cluster based on Euclidean distances. Marker genes that were significantly enriched for each cluster were then identified, allowing cluster annotation to specific cell types. After removing the contaminant cell cluster (i.e., red blood cells and retinal pigmented epithelium), a total of 13,638 cells were obtained from normoxic retina (9191 from whole retina and 4447 from rod-depleted retina) and 17,473 cells from OIR retina (11,732 from whole retina and 5741 from rod-depleted retina). Transcriptomic differences between normoxic and OIR cell types were statistically compared using a negative binomial model and analyzed using visualization tools including Dot Plot, RidgePlot, t-SNE plot, and heatmap plot. For pathway analysis, normalized single-cell gene expression profiles from each separate cell type identified by scRNAseq (downsampled to a maximum of 1000 cells per cell cluster) were further analyzed using GSVA (*87*). Single-cell gene expression profiles from each separate cell type identified by scRNAseq were further analyzed using CellPhoneDB (*49*). The data discussed herein have been deposited in NCBI's Gene Expression Omnibus (accession no. GSE150703).

Human neutrophil isolation

Blood was drawn from healthy volunteers in accordance with HMR guidelines. Neutrophil isolation was performed using a published protocol. Briefly, red blood cells were first removed with an Histopaque 1119 gradient. The top leukocyte fraction was separated with a 65-70-75-80-85% Percoll gradient. Neutrophils were collected in the fractions above 70%. Cells were washed twice with phosphate-buffered saline (PBS) and counted using an hemacytometer.

Time-lapse microscopy

ECs (HUVEC, Lonza) were transduced with an RAS expressing or empty plasmid retrovirus for 2 rounds of 6-hour incubations. RAS-expressing ECs were selected after 5 days of selection with 100 μg/ml of hygromycin. Control and senescent cells were seeded in a 96-well plate the day before. Human neutrophils were isolated as described previously, labeled for 20 min with 1 uM DiI Red at 37°C, washed twice, and added to the EC layer along with Sytox Green (150 nM). Images were acquired using a Zeiss Z1 live microscope equipped with a humidified chamber at 37°C at 5-min intervals. Image analysis was done using Imaris software. For imaging in live retinas, cardiac perfusion was done with 5 μg of Ly6G-FITC antibody (BioLegend) and 20 μg of lectin-rhodamine (Vector Laboratories) in mouse pups at P17 of OIR. Eyes were quickly removed and placed on ice in Ringer's solution. Retinas were dissected, flattened out on 0.4-μm cell culture inserts (Millipore), and kept humidified at all times in Ringer's solution. Images were acquired with a multiphoton Zeiss LSM880 microscope and Zeiss Zen Black software.

Lentivirus and adenovirus production

For lentivirus production, HEK293T cells were transfected with third-generation packaging plasmids (12251, 12253, and 12259, Addgene) using polyethylenimine. Lentiviruses were collected in the supernatants after 56 hours. Supernatants were cleared by centrifugation and filtered through 0.45-μm filters to remove cell debris. For retrovirus production, Phoenix-AMPHO cells were transfected with either pWZL-HYGRO or pWZL-HYGRO-RASV12 in complete Dulbecco's modified Eagle's medium (DMEM). Thirty to 36 hours after transfection, the medium was replaced and incubated for a further 12 to 16 hours. Viruses were harvested, Phoenix-AMPHO cells were replenished with fresh DMEM for 12 hours, and viruses were collected a second time. Phoenix-AMPHO cells were purchased from ATCC (Manassas, VA, USA).

Real-time PCR analysis

RNA was isolated using the GenElute Mammalian Total RNA Miniprep Kit (Sigma-Aldrich) and further digested with DNase I to prevent amplification of genomic DNA. RNA was reverse transcribed using M-MLV reverse transcriptase and gene expression was analyzed using SYBR Green in an ABI Biosystems Real-Time PCR machine. β-actin was used as a reference gene. All primer sequences can be found in fig. S19.

FACS of digested retinas

Retinas from pups' eyes were dissected and homogenized with a solution of 750U/ml DNaseI (Sigma-Aldrich) and 0.5 mg/ml of collagenase D (Roche) for 15 min at 37°C with gentle shaking. Homogenates were then filtered with a 70-μm cell strainer and washed in RPMI plus 2% fetal bovine serum. Blocking was done with an FC block (CD16/CD32) from BioLegend. A cocktail of anti-CD45.2, anti-CD11b, anti-CX3CR1, anti-CD3ε, anti-Ly6C, anti-Ly6G, or anti-F4/80, and anti-Gr1 antibodies was used, as well as 7-amino-actinomycin D for detection of neutrophils. Analysis was performed using a FACSCanto flow cytometer (BD Biosciences) and the FlowJo version 7.6 software.

Immunohistochemistry

Eyes were enucleated from mice and fixed in 4% paraformaldehyde before incubation in 30% sucrose and inclusion in optimal cutting temperature medium. Serial sections (12 μm) were taken, visualized using a confocal microscope (Olympus FV1000), and stained with 4′,6-diamidino-2-phenylindole (DAPI) and lectin-rhodamine.

MPO detection

Retinas from mice at various time points throughout OIR or during normal development were homogenized and the activity of the specific neutrophil peroxydase MPO was measured using O-dianisidine as a substrate. Briefly, retinas were homogenized in 50 mM potassium phosphate buffer, pH 6.0, containing 0.5% hexadecyltrimethylammonium bromide (HETAB), sonicated, and freeze-thawed for three cycles. The homogenates were centrifuged for 20 min at 20,000*g*. Analysis of MPO activity of the supernatants was done using a 50 mM potassium phosphate buffer, pH 6.0, containing 0.167 mg/ml O-dianisidine hydrochloride and 0.0005% H_2O_2. Absorbance was measured at 460nm at 25°C.

dsDNA and elastase activity quantification in human vitreous

dsDNA was detected in the vitreous using the PicoGreen dsDNA reagent (Invitrogen) according to the manufacturer's instructions. Elastase activity was assessed with human neutrophil elastase substrate N-succinyl-Ala-Ala-Ala-p-nitroanilide (Sigma-Aldrich) and recorded at 405 nm for a period of 60 min.

SA-β-Gal activity

For quantification of SA-β-Gal activity, cells or retinas were washed twice in PBS and fixed with 4% PFA for 15 min or 1 hour (retinas). After two washes in PBS with 1 mM $MgCl_2$ (adjusted to pH 5.0 for mouse retinas or 6.0 for HUVEC), incubation was done overnight in KC solution {5 mM $K3[Fe(CN)_6]$ + 6mM $K_4[Fe(CN)_6]$ in PBS with 1 mM $MgCl_2$ with adjusted pH and 1 mg/ml X-Gal substrate}. Photographs were taken with a Zeiss AxioObserver Z1 motorized inverted microscope using Zeiss Blue Software.

SILAC

HUVEC cells were grown in Lys/Arg free Iscove's modified Dulbecco's medium resupplemented with heavy or light Lys and Arg for a minimum of four population doublings before induction of senescence with retroviral expression of RASV12 or empty vector. Selection was performed with 100 μg/ml of hygromycin. At 10 days after the induction of senescence, cells were incubated in serum-free medium and supernatants collected after 24 hours. Proteins were precipitated using acetone at −20°C for 1 hour and resuspended in 8 M urea and 20 mM HEPES, pH 8.0. The extracted proteins were then digested, mixed in equal proportions, and analyzed by MS. Postanalysis was done with MaxQuant software. Incorporation of heavy and light isotopes was estimated to be >90%.

Statistical analyses

Data are presented as mean ± SEM. Student's *t* test or ANOVA was used to compare the different groups. $P < 0.05$ was considered statistically different.

REFERENCES AND NOTES

1. R. Lee, T. Y. Wong, C. Sabanayagam, Epidemiology of diabetic retinopathy, diabetic macular edema and related vision loss. *Eye Vis.* **2**, 17 (2015). doi: 10.1186/s40662-015-0026-2; pmid: 26605370
2. J. Ding, T. Y. Wong, Current epidemiology of diabetic retinopathy and diabetic macular edema. *Curr. Diab. Rep.* **12**, 346–354 (2012). doi: 10.1007/s11892-012-0283-6; pmid: 22585044
3. E. J. Duh, J. K. Sun, A. W. Stitt, Diabetic retinopathy: Current understanding, mechanisms, and treatment strategies. *JCI Insight* **2**, e93751 (2017). doi: 10.1172/jci.insight.93751; pmid: 28724805
4. J. H. Kempen *et al*., The prevalence of diabetic retinopathy among adults in the United States. *Arch. Ophthalmol.* **122**, 552–563 (2004). doi: 10.1001/archopht.122.4.552; pmid: 15078674
5. A. Hellström, L. E. Smith, O. Dammann, Retinopathy of prematurity. *Lancet* **382**, 1445–1457 (2013). doi: 10.1016/S0140-6736(13)60178-6; pmid: 23782686
6. M. E. Hartnett, J. S. Penn, Mechanisms and management of retinopathy of prematurity. *N. Engl. J. Med.* **367**, 2515–2526 (2012). doi: 10.1056/NEJMra1208129; pmid: 23268666
7. E. H. Lo, A new penumbra: Transitioning from injury into repair after stroke. *Nat. Med.* **14**, 497–500 (2008). doi: 10.1038/nm1735; pmid: 18463660
8. M. A. Moskowitz, E. H. Lo, C. Iadecola, The science of stroke: Mechanisms in search of treatments. *Neuron* **67**, 181–198 (2010). doi: 10.1016/j.neuron.2010.07.002; pmid: 20670828
9. P. Sapieha, Eyeing central neurons in vascular growth and reparative angiogenesis. *Blood* **120**, 2182–2194 (2012). doi: 10.1182/blood-2012-04-396846; pmid: 22705597
10. C. A. K. Lange, J. W. B. Bainbridge, Oxygen sensing in retinal health and disease. *Ophthalmologica* **227**, 115–131 (2012). pmid: 21952513
11. M. Oubaha *et al*., Senescence-associated secretory phenotype contributes to pathological angiogenesis in retinopathy. *Sci. Transl. Med.* **8**, 362ra144 (2016). doi: 10.1126/scitranslmed.aaf9440; pmid: 27797960
12. National Eye Institute, National Institutes of Health, At a glance: Retinopathy of prematurity 2014); www.nei.nih.gov/learn-about-eye-health/eye-conditions-and-diseases/retinopathy-prematurity.
13. F. Bandello, J. D. Gass, R. Lattanzio, R. Brancato, Spontaneous regression of neovascularization at the disk and elsewhere in diabetic retinopathy. *Am. J. Ophthalmol.* **122**, 494–501 (1996). doi: 10.1016/S0002-9394(14)72108-7; pmid: 8862045

14. J. R. Han, W. K. Ju, I. W. Park, Spontaneous regression of neovascularization at the disc in diabetic retinopathy. *Korean J. Ophthalmol.* **18**, 41–46 (2004). doi: 10.3341/kjo.2004.18.1.41; pmid: 15255236
15. H. L. Little, Treatment of proliferative diabetic retinopathy. Long-term results of argon laser photocoagulation. *Ophthalmology* **92**, 279–283 (1985). doi: 10.1016/S0161-6420(85)34059-9; pmid: 2580259
16. R. L. Avery *et al*., Intravitreal bevacizumab (Avastin) in the treatment of proliferative diabetic retinopathy. *Ophthalmology* **113**, 1695.e1–1695.e15 (2006). doi: 10.1016/j.ophtha.2006.05.064; pmid: 17011951
17. Y. Yoshikawa *et al*., Developmental regression of hyaloid vasculature is triggered by neurons. *J. Exp. Med.* **213**, 1175–1183 (2016). doi: 10.1084/jem.20151966; pmid: 27325890
18. I. B. Lobov *et al*., WNT7b mediates macrophage-induced programmed cell death in patterning of the vasculature. *Nature* **437**, 417–421 (2005). doi: 10.1038/nature03928; pmid: 16163358
19. G. A. Lutty, D. S. McLeod, Development of the hyaloid, choroidal and retinal vasculatures in the fetal human eye. *Prog. Retin. Eye Res.* **62**, 58–76 (2018). doi: 10.1016/j.preteyeres.2017.10.001; pmid: 29081352
20. S. E. Hamrick, G. Hansmann, Patent ductus arteriosus of the preterm infant. *Pediatrics* **125**, 1020–1030 (2010). doi: 10.1542/peds.2009-3506; pmid: 20421261
21. J. E. Girling, P. A. Rogers, Regulation of endometrial vascular remodeling: Role of the vascular endothelial growth factor family and the angiopoietin-TIE signalling system. *Reproduction* **138**, 883–893 (2009). doi: 10.1530/REP-09-0147; pmid: 19755482
22. D. F. Gilmour, Familial exudative vitreoretinopathy and related retinopathies. *Eye* (*Lond.*) **29**, 1–14 (2015). doi: 10.1038/eye.2014.70; pmid: 25323851
23. E. R. Hermes-DeSantis, R. I. Clyman, Patent ductus arteriosus: Pathophysiology and management. *J. Perinatol.* **26** (Suppl 1), S14–S18, discussion S22–S23 (2006). doi: 10.1038/sj.jp.7211465; pmid: 16625216
24. D. S. Torry, R. J. Torry, Angiogenesis and the expression of vascular endothelial growth factor in endometrium and placenta. *Am. J. Reprod. Immunol.* **37**, 21–29 (1997). doi: 10.1111/j.1600-0897.1997.tb00189.x; pmid: 9138450
25. H. P. Gerber, N. Ferrara, Pharmacology and pharmacodynamics of bevacizumab as monotherapy or in combination with cytotoxic therapy in preclinical studies. *Cancer Res.* **65**, 671–680 (2005). pmid: 15705858
26. R. K. Jain, Normalization of tumor vasculature: An emerging concept in antiangiogenic therapy. *Science* **307**, 58–62 (2005). doi: 10.1126/science.1104819; pmid: 15637262
27. R. S. Apte, D. S. Chen, N. Ferrara, VEGF in signaling and disease: Beyond discovery and development. *Cell* **176**, 1248–1264 (2019). doi: 10.1016/j.cell.2019.01.021; pmid: 30849371
28. L. E. Smith *et al*., Oxygen-induced retinopathy in the mouse. *Invest. Ophthalmol. Vis. Sci.* **35**, 101–111 (1994). pmid: 7507904
29. F. Binet *et al*., Neuronal ER stress impedes myeloid-cell-induced vascular regeneration through IRE1α degradation of netrin-1. *Cell Metab.* **17**, 353–371 (2013). doi: 10.1016/j.cmet.2013.02.003; pmid: 23473031
30. E. Z. Macosko *et al*., Highly parallel genome-wide expression profiling of individual cells using nanoliter droplets. *Cell* **161**, 1202–1214 (2015). doi: 10.1016/j.cell.2015.05.002; pmid: 26000488
31. D. Aran *et al*., Reference-based analysis of lung single-cell sequencing reveals a transitional profibrotic macrophage. *Nat. Immunol.* **20**, 163–172 (2019). doi: 10.1038/s41590-018-0276-y; pmid: 30643263
32. D. Checchin, F. Sennlaub, E. Levavasseur, M. Leduc, S. Chemtob, Potential role of microglia in retinal blood vessel formation. *Invest. Ophthalmol. Vis. Sci.* **47**, 3595–3602 (2006). doi: 10.1167/iovs.05-1522; pmid: 16877434
33. Y. Kubota *et al*., M-CSF inhibition selectively targets pathological angiogenesis and lymphangiogenesis. *J. Exp. Med.* **206**, 1089–1102 (2009). doi: 10.1084/jem.20081605; pmid: 19398755
34. M. R. Ritter *et al*., Myeloid progenitors differentiate into microglia and promote vascular repair in a model of ischemic retinopathy. *J. Clin. Invest.* **116**, 3266–3276 (2006). doi: 10.1172/JCI29683; pmid: 17111048
35. B. W. Bardoel, E. F. Kenny, G. Sollberger, A. Zychlinsky, The balancing act of neutrophils. *Cell Host Microbe* **15**, 526–536 (2014). doi: 10.1016/j.chom.2014.04.011; pmid: 24832448
36. B. McDonald, P. Kubes, Chemokines: Sirens of neutrophil recruitment-but is it just one song? *Immunity* **33**, 148–149 (2010). doi: 10.1016/j.immuni.2010.08.006; pmid: 20732637
37. V. Papayannopoulos, Neutrophil extracellular traps in immunity and disease. *Nat. Rev. Immunol.* **18**, 134–147 (2018). doi: 10.1038/nri.2017.105; pmid: 28990587
38. A. S. Rohrbach, D. J. Slade, P. R. Thompson, K. A. Mowen, Activation of PAD4 in NET formation. *Front. Immunol.* **3**, 360 (2012). doi: 10.3389/fimmu.2012.00360; pmid: 23264775
39. A. Warnatsch, M. Ioannou, Q. Wang, V. Papayannopoulos, Neutrophil extracellular traps license macrophages for cytokine production in atherosclerosis. *Science* **349**, 316–320 (2015). doi: 10.1126/science.aaa8064; pmid: 26185250
40. H. Huang *et al*., Damage-associated molecular pattern-activated neutrophil extracellular trap exacerbates sterile inflammatory liver injury. *Hepatology* **62**, 600–614 (2015). doi: 10.1002/hep.27841; pmid: 25855125
41. V. Papayannopoulos, K. D. Metzler, A. Hakkim, A. Zychlinsky, Neutrophil elastase and myeloperoxidase regulate the formation of neutrophil extracellular traps. *J. Cell Biol.* **191**, 677–691 (2010). doi: 10.1083/jcb.201006052; pmid: 20974816
42. M. Pearson *et al*., PML regulates p53 acetylation and premature senescence induced by oncogenic Ras. *Nature* **406**, 207–210 (2000). doi: 10.1038/35018127; pmid: 10910364
43. G. Ferbeyre *et al*., PML is induced by oncogenic ras and promotes premature senescence. *Genes Dev.* **14**, 2015–2027 (2000). pmid: 10950866
44. A. Hernandez-Segura, J. Nehme, M. Demaria, Hallmarks of cellular senescence. *Trends Cell Biol.* **28**, 436–453 (2018). doi: 10.1016/j.tcb.2018.02.001; pmid: 29477613
45. M. Serrano, A. W. Lin, M. E. McCurrach, D. Beach, S. W. Lowe, Oncogenic ras provokes premature cell senescence associated with accumulation of p53 and p16INK4a. *Cell* **88**, 593–602 (1997). doi: 10.1016/S0092-8674(00)81902-9; pmid: 9054499
46. R. Di Micco *et al*., Oncogene-induced senescence is a DNA damage response triggered by DNA hyper-replication. *Nature* **444**, 638–642 (2006). doi: 10.1038/nature05327; pmid: 17136094
47. F. A. Mallette, M. F. Gaumont-Leclerc, G. Ferbeyre, The DNA damage signaling pathway is a critical mediator of oncogene-induced senescence. *Genes Dev.* **21**, 43–48 (2007). doi: 10.1101/gad.1487307; pmid: 17210786
48. J. Bartkova *et al*., Oncogene-induced senescence is part of the tumorigenesis barrier imposed by DNA damage checkpoints. *Nature* **444**, 633–637 (2006). doi: 10.1038/nature05268; pmid: 17136093
49. M. Efremova, M. Vento-Tormo, S. A. Teichmann, R. Vento-Tormo, CellPhoneDB: Inferring cell-cell communication from combined expression of multi-subunit ligand-receptor complexes. *Nat. Protoc.* **15**, 1484–1506 (2020). doi: 10.1038/s41596-020-0292-x; pmid: 32103204
50. P. D. Westenskow *et al*., Ras pathway inhibition prevents neovascularization by repressing endothelial cell sprouting. *J. Clin. Invest.* **123**, 4900–4908 (2013). doi: 10.1172/JCI70230; pmid: 24084735
51. A. Fabregat *et al*., Reactome diagram viewer: Data structures and strategies to boost performance. *Bioinformatics* **34**, 1208–1214 (2018). doi: 10.1093/bioinformatics/btx752; pmid: 29186351
52. J. C. Acosta *et al*., A complex secretory program orchestrated by the inflammasome controls paracrine senescence. *Nat. Cell Biol.* **15**, 978–990 (2013). doi: 10.1038/ncb2784; pmid: 23770676
53. J. P. Coppé, P. Y. Desprez, A. Krtolica, J. Campisi, The senescence-associated secretory phenotype: The dark side of tumor suppression. *Annu. Rev. Pathol.* **5**, 99–118 (2010). doi: 10.1146/annurev-pathol-121808-102144; pmid: 20078217
54. M. Saffarzadeh *et al*., Neutrophil extracellular traps directly induce epithelial and endothelial cell death: A predominant role of histones. *PLOS ONE* **7**, e32366 (2012). doi: 10.1371/journal.pone.0032366; pmid: 22389696
55. A. K. Gupta *et al*., Activated endothelial cells induce neutrophil extracellular traps and are susceptible to NETosis-mediated cell death. *FEBS Lett.* **584**, 3193–3197 (2010). doi: 10.1016/j.febslet.2010.06.006; pmid: 20541553
56. P. Li *et al*., PAD4 is essential for antibacterial innate immunity mediated by neutrophil extracellular traps. *J. Exp. Med.* **207**, 1853–1862 (2010). doi: 10.1084/jem.20100239; pmid: 20733033
57. A. Hakkim *et al*., Impairment of neutrophil extracellular trap degradation is associated with lupus nephritis. *Proc. Natl. Acad. Sci. U.S.A.* **107**, 9813–9818 (2010). doi: 10.1073/pnas.0909927107; pmid: 20439745
58. J. M. Daley, A. A. Thomay, M. D. Connolly, J. S. Reichner, J. E. Albina, Use of Ly6G-specific monoclonal antibody to deplete neutrophils in mice. *J. Leukoc. Biol.* **83**, 64–70 (2008). doi: 10.1189/jlb.0407247; pmid: 17884993
59. A. Stahl *et al*., The mouse retina as an angiogenesis model. *Invest. Ophthalmol. Vis. Sci.* **51**, 2813–2826 (2010). doi: 10.1167/iovs.10-5176; pmid: 20484600
60. S. Lavalette *et al*., Interleukin-1β inhibition prevents choroidal neovascularization and does not exacerbate photoreceptor degeneration. *Am. J. Pathol.* **178**, 2416–2423 (2011). doi: 10.1016/j.ajpath.2011.01.013; pmid: 21514452
61. J. C. Rivera *et al*., Microglia and interleukin-1β in ischemic retinopathy elicit microvascular degeneration through neuronal semaphorin-3A. *Arterioscler. Thromb. Vasc. Biol.* **33**, 1881–1891 (2013). doi: 10.1161/ATVBAHA.113.301331; pmid: 23766263
62. P. Sapieha, F. A. Mallette, Cellular senescence in postmitotic cells: Beyond growth arrest. *Trends Cell Biol.* **28**, 595–607 (2018). doi: 10.1016/j.tcb.2018.03.003; pmid: 29704982
63. D. Muñoz-Espín, M. Serrano, Cellular senescence: From physiology to pathology. *Nat. Rev. Mol. Cell Biol.* **15**, 482–496 (2014). doi: 10.1038/nrm3823; pmid: 24954210
64. J. Campisi, F. d'Adda di Fagagna, Cellular senescence: When bad things happen to good cells. *Nat. Rev. Mol. Cell Biol.* **8**, 729–740 (2007). doi: 10.1038/nrm2233; pmid: 17667954
65. M. Demaria *et al*., An essential role for senescent cells in optimal wound healing through secretion of PDGF-AA. *Dev. Cell* **31**, 722–733 (2014). doi: 10.1016/j.devcel.2014.11.012; pmid: 25499914
66. L. Mosteiro *et al*., Tissue damage and senescence provide critical signals for cellular reprogramming in vivo. *Science* **354**, aaf4445 (2016). doi: 10.1126/science.aaf4445; pmid: 27884981
67. B. Ritschka *et al*., The senescence-associated secretory phenotype induces cellular plasticity and tissue regeneration. *Genes Dev.* **31**, 172–183 (2017). doi: 10.1101/gad.290635.116; pmid: 28143833
68. T. W. Kang *et al*., Senescence surveillance of pre-malignant hepatocytes limits liver cancer development. *Nature* **479**, 547–551 (2011). doi: 10.1038/nature10599; pmid: 22080947
69. V. Krizhanovsky *et al*., Implications of cellular senescence in tissue damage response, tumor suppression, and stem cell biology. *Cold Spring Harb. Symp. Quant. Biol.* **73**, 513–522 (2008). doi: 10.1101/sqb.2008.73.048; pmid: 19150958
70. W. Xue *et al*., Senescence and tumour clearance is triggered by p53 restoration in murine liver carcinomas. *Nature* **445**, 656–660 (2007). doi: 10.1038/nature05529; pmid: 17251933
71. J. H. Sweigard *et al*., The alternative complement pathway regulates pathological angiogenesis in the retina. *FASEB J.* **28**, 3171–3182 (2014). doi: 10.1096/fj.14-251041; pmid: 24668752
72. M. H. Davies, A. J. Stempel, M. R. Powers, MCP-1 deficiency delays regression of pathologic retinal neovascularization in a model of ischemic retinopathy. *Invest. Ophthalmol. Vis. Sci.* **49**, 4195–4202 (2008). doi: 10.1167/iovs.07-1491; pmid: 18487365
73. A. Sagiv *et al*., NKG2D ligands mediate immunosurveillance of senescent cells. *Aging* (*Albany NY*) **8**, 328–344 (2016). doi: 10.18632/aging.100897; pmid: 26878797
74. M. H. Yun, H. Davaapil, J. P. Brockes, Recurrent turnover of senescent cells during regeneration of a complex structure. *eLife* **4**, e05505 (2015). doi: 10.7554/eLife.05505; pmid: 25942455
75. K. Kessenbrock *et al*., Netting neutrophils in autoimmune small-vessel vasculitis. *Nat. Med.* **15**, 623–625 (2009). doi: 10.1038/nm.1959; pmid: 19448636
76. G. Li *et al*., Marrow-derived cells regulate the development of early diabetic retinopathy and tactile allodynia in mice. *Diabetes* **61**, 3294–3303 (2012). doi: 10.2337/db11-1249; pmid: 22923475
77. A. A. Veenstra, J. Tang, T. S. Kern, Antagonism of CD11b with neutrophil inhibitory factor (NIF) inhibits vascular lesions in diabetic retinopathy. *PLOS ONE* **8**, e78405 (2013). doi: 10.1371/journal.pone.0078405; pmid: 24205223
78. S. J. Woo, S. J. Ahn, J. Ahn, K. H. Park, K. Lee, Elevated systemic neutrophil count in diabetic retinopathy and diabetes: A hospital-based cross-sectional study of 30,793 Korean subjects. *Invest. Ophthalmol. Vis. Sci.* **52**, 7697–7703 (2011). doi: 10.1167/iovs.11-7784; pmid: 21873679
79. J. O. Chung, S. Y. Park, D. H. Cho, D. J. Chung, M. Y. Chung, Plasma neutrophil gelatinase-associated lipocalin levels are positively associated with diabetic retinopathy in patients with Type 2 diabetes. *Diabet. Med.* **33**, 1649–1654 (2016). doi: 10.1111/dme.13141; pmid: 27100138

80. S. Y. Kim *et al*., Neutrophils are associated with capillary closure in spontaneously diabetic monkey retinas. *Diabetes* **54**, 1534–1542 (2005). doi: 10.2337/diabetes.54.5.1534; pmid: 15855343
81. J. H. Park *et al*., Evaluation of circulating markers of neutrophil extracellular trap (NET) formation as risk factors for diabetic retinopathy in a case-control association study. *Exp. Clin. Endocrinol. Diabetes* **124**, 557–561 (2016). doi: 10.1055/s-0042-101792; pmid: 27420129
82. L. Boneschansker, Y. Inoue, R. Oklu, D. Irimia, Capillary plexuses are vulnerable to neutrophil extracellular traps. *Integr. Biol.* (*Camb.*) **8**, 149–155 (2016). doi: 10.1039/C5IB00265F; pmid: 26797289

ACKNOWLEDGMENTS

We thank M. Sergeev, M. Lambert, and N. Tessier for their helpful assistance. **Funding:** This work was supported by operating grants from the Canadian Diabetes Association (grant DI-3-18-5444-PS to P.S.), the Canadian Institutes of Health Research (foundation grant 148460 to P.S.; grant PJ2-169643 to F.A.M. and P.S., grants 141956 and 390615 to J.-S. J., grant MOP-133442 to F.A.M.; grant GER-163050 to F.A.M. and K.B.; and grant MOP142425 to J.-F.C.), the Canadian the Heart & Stroke Foundation Canada (grant G-16-00014658 to P.S. and F.A.M.), the Foundation Fighting Blindness Canada (grant to P.S. and J.-S.J.), and the Natural Sciences and Engineering Research Council of Canada (grant 418637 to P.S., grant RGPIN-2017-05227 to F.A.M., and grant RGPIN-2016-06743 to J.-S.J.). P.S. holds the Wolfe Professorship in Translational Research and a Canada Research Chair in Retinal Cell Biology. F.A.M. is the recipient of the Canada Research Chair in Epigenetics of Aging and Cancer. J.-S.J. was supported by the Burroughs Wellcome Fund Career Award for Medical Scientists (grant 1012321.01) and the Fonds de Recherche du Québec - Santé (FRQS). J.-F.C, holds the TRANSAT Chair in breast cancer research. F.B., S.C.-G., G.T.M., and A.A.T. received fellowships from the FRQS. G.C. holds a MITACs postdoctoral fellowship and is funded by the Single-Cell Academy (The Vision Health Research Network of Quebec (RRSV)) and the Antoine Turmel Foundation. M.H. holds the Banting Fellowship from the CIHR. R.D. and G.T.M. hold scholarships from the Fonds de Recherche en Ophtalmologie de l'Université de Montréal (FROUM) and the RRSV. M.N. obtained fellowships from FRQS and the Cole Foundation. C.S. obtained PhD studentships from the Cole Foundation, FRQS, and Hydro-Québec. K.B. obtained a fellowship from the Cole Foundation. **Author contributions:** P.S., F.B., and F.A.M. designed the research and study. J.S.J., G.C., S.L., J.P.H., and G.A. carried out single-cell RNAseq work. F.B., A.D., M.N., M.H., A.W., V.G., M.B., R.L., S.C.-G., G.T.M., C.S., R.D., C.P., R.J., F.P., K.B., and A.A.T. carried out experimental work. F.A.R. performed all retinal surgeries. F.B., G.C., J.P.H., M.B., A.A.T., and J.F.C. analyzed the data. F.S. provided valuable insight on research design. P.S., F.B., and F.A.M. wrote the manuscript with valuable input from all authors. **Competing interests:** P.S. is a consultant for UNITY Biotechnology. **Data and materials availability:** All single-cell data for the study are deposited in NCBI's Gene Expression Omnibus and are accessible through GEO accession no. GSE150703. All bulk RNAseq data and gene sets used are available in the supplementary materials.

SUPPLEMENTARY MATERIALS

science.sciencemag.org/content/369/6506/eaay5356/suppl/DC1
Figs. S1 to S19
Table S1
Reproducibility Checklist
Movie S1
Databases S1 to S6

View/request a protocol for this paper from *Bio-protocol*.

27 June 2019; resubmitted 17 May 2020
Accepted 6 July 2020
10.1126/science.aay5356

Science

Neutrophil extracellular traps target senescent vasculature for tissue remodeling in retinopathy

François Binet, Gael Cagnone, Sergio Crespo-Garcia, Masayuki Hata, Mathieu Neault, Agnieszka Dejda, Ariel M. Wilson, Manuel Buscarlet, Gaelle Tagne Mawambo, Joel P. Howard, Roberto Diaz-Marin, Celia Parinot, Vera Guber, Frédérique Pilon, Rachel Juneau, Rémi Laflamme, Christina Sawchyn, Karine Boulay, Severine Leclerc, Afnan Abu-Thuraia, Jean-François Côté, Gregor Andelfinger, Flavio A. Rezende, Florian Sennlaub, Jean-Sébastien Joyal, Frédérick A. Mallette and Przemyslaw Sapieha

Science **369** (6506), eaay5356.
DOI: 10.1126/science.aay5356

Remodeling senescent blood vessels

The retina is a thin layer of nervous tissue at the back of the eye that transforms light into neuronal signals. The retina is essential for vision and is supported by networks of blood vessels. In diabetic retinopathy, a common cause of vision loss, these microvessels degenerate and regrow in an aberrant manner. Such degeneration and regrowth can compromise the functioning of retinal nerve cells. Binet *et al.* observed that, after rapid proliferation, vascular endothelial cells in diseased blood vessels engaged molecular pathways linked to cellular senescence (see the Perspective by Podrez and Byzova). Senescent vascular units summoned an inflammatory response in which neutrophils extruded neutrophil extracellular traps onto diseased vessels to remodel them. This endogenous repair mechanism promoted the elimination of senescent blood vessels and could lead to beneficial vascular remodeling.

Science, this issue p. eaay5356; see also p. 919

Science (print ISSN 0036-8075; online ISSN 1095-9203) is published by the American Association for the Advancement of Science, 1200 New York Avenue NW, Washington, DC 20005. The title *Science* is a registered trademark of AAAS.